Performance report of the RHUM-RUM ocean bottom seismometer network around La Réunion, western Indian Ocean

Journal Article

Author(s):
Stähler, Simon Christian; Sigloch, Karin; Hosseini, Kasra; Crawford, Wayne C.; Barruol, Guilhem; Schmidt-Aursch, Mechita C.; Tsekhmistrenko, Maria; Scholz, John R.; Mazzullo, Alessandro; Deen, Martha

Publication date:
2016-02-02

Permanent link:
https://doi.org/10.3929/ethz-b-000286172

Originally published in:
Advances in Geosciences 41, https://doi.org/10.5194/adgeo-41-43-2016

Adv. Geosci., 41, 43–63, 2016
www.adv-geosci.net/41/43/2016/
doi:10.5194/adgeo-41-43-2016

Advances in Geosciences
Open Access
EGU

Performance report of the RHUM-RUM ocean bottom seismometer network around La Réunion, western Indian Ocean

S. C. Stähler[1,6], K. Sigloch[2,1], K. Hosseini[1], W. C. Crawford[3], G. Barruol[4], M. C. Schmidt-Aursch[5], M. Tsekhmistrenko[2,5], J.-R. Scholz[4,5], A. Mazzullo[3], and M. Deen[3]

[1]Dept. of Earth Sciences, Ludwig-Maximilians-Universität München, Theresienstrasse 41, 80333 Munich, Germany
[2]Dept. of Earth Sciences, University of Oxford, South Parks Road, Oxford, OX1 3AN, UK
[3]Institut de Physique du Globe de Paris, Sorbonne Paris Cité, UMR7154 – CNRS, Paris, France
[4]Laboratoire GéoSciences Réunion, Université de La Réunion, Institut de Physique du Globe de Paris, Sorbonne Paris Cité, UMR7154 – CNRS, Université Paris Diderot, Saint Denis CEDEX 9, France
[5]Alfred Wegener Institute, Helmholtz Centre for Polar and Marine Research, Am Alten Hafen 26, 27568 Bremerhaven, Germany
[6]Leibniz-Institute for Baltic Sea Research, Seestraße 15, 18119 Rostock, Germany

Correspondence to: S. Stähler (staehler@geophysik.uni-muenchen.de)

Received: 21 July 2015 – Revised: 23 December 2015 – Accepted: 21 January 2016 – Published: 2 February 2016

Abstract. RHUM-RUM is a German-French seismological experiment based on the sea floor surrounding the island of La Réunion, western Indian Ocean (Barruol and Sigloch, 2013). Its primary objective is to clarify the presence or absence of a mantle plume beneath the Reunion volcanic hotspot. RHUM-RUM's central component is a 13-month deployment (October 2012 to November 2013) of 57 broadband ocean bottom seismometers (OBS) and hydrophones over an area of $2000 \times 2000\,\mathrm{km}^2$ surrounding the hotspot. The array contained 48 wideband OBS from the German DEPAS pool and 9 broadband OBS from the French INSU pool. It is the largest deployment of DEPAS and INSU OBS so far, and the first joint experiment.

This article reviews network performance and data quality: of the 57 stations, 46 and 53 yielded good seismometer and hydrophone recordings, respectively. The 19 751 total deployment days yielded 18 735 days of hydrophone recordings and 15 941 days of seismometer recordings, which are 94 and 80 % of the theoretically possible yields.

The INSU seismic sensors stand away from their OBS frames, whereas the DEPAS sensors are integrated into their frames. At long periods ($> 10\,\mathrm{s}$), the DEPAS seismometers are affected by significantly stronger noise than the INSU seismometers. On the horizontal components, this can be explained by tilting of the frame and buoy assemblage, e.g. through the action of ocean-bottom currents, but in addition the DEPAS intruments are affected by significant self-noise at long periods, including on the vertical channels. By comparison, the INSU instruments are much quieter at periods $> 30\,\mathrm{s}$ and hence better suited for long-period signals studies.

The trade-off of the instrument design is that the integrated DEPAS setup is easier to deploy and recover, especially when large numbers of stations are involved. Additionally, the wideband sensor has only half the power consumption of the broadband INSU seismometers. For the first time, this article publishes response information of the DEPAS instruments, which is necessary for any project where true ground displacement is of interest. The data will become publicly available at the end of 2017.

1 Introduction

RHUM-RUM, short for "Reunion Hotspot and Upper Mantle – Réunions Unterer Mantel", is a German-French experiment that investigates the mantle beneath the Reunion ocean island hotspot from crust to core, using a multitude of seismological and marine geophysical methods (Barruol and Sigloch, 2013). The project also studies the hypothesized interaction between the hotspot and its surrounding mid-ocean ridges (Morgan, 1978; Dyment et al., 2007). The core of the exper-

iment is a deployment of 48 German wideband and 9 French broadband ocean-bottom seismometers (OBS), from the DEPAS (Deutscher Geräte-Pool für Amphibische Seismologie, managed by AWI Bremerhaven) and INSU (Institut national des sciences de l'Univers) pools respectively (see Table 1 for the data return).

There have been multiple experiments in tectonic settings similar to RHUM-RUM: 35 wideband and broadband OBS from the US OBS Instrument Pool (OBSIP) were deployed by the PLUME Hawaii experiment (Laske et al., 2009; Wolfe et al., 2009) twice for 1 year. Japanese large-scale imaging efforts around an oceanic hotspot were the PLUME Tahiti experiment with 9 Japanese broadband OBS (BBOBS) (Barruol, 2002; Suetsugu et al., 2005) and the TIARES array with again 9 BBOBS around the Society hotspot (Suetsugu et al., 2012). In 2011–2012, 24 German DEPAS OBS were deployed around the Tristan da Cunha hotspot (ISOLDE experiment, Geissler and Schmidt, 2013). Other larger, long-term DEPAS deployments in non-hotspot settings were in the Aegean Sea (EGELADOS, Meier et al., 2007) and in the Gulf of Cadiz (NEAREST, Geissler et al., 2010).

RHUM-RUM has been the largest DEPAS deployment so far in terms of the number of stations deployed ($44 + 4$) and in terms of aperture. This allows to resolve the deep-mantle signature of a plume using seismic tomography, especially when combined with concurrent land deployments. It is the first OBS experiment that specifically tries to use data for waveform tomography. This requires full response information on all instruments and also a high signal-to-noise ratio in the whole frequency range between 0.01 and 1 Hz.

The central component of the experiment was a deployment of 44 wideband OBS from DEPAS, of the so-called "LOBSTER" (Longterm OBS for Tsunami and Earthquake Research) type; 4 from Geomar Kiel, essentially identical to the DEPAS LOBSTERs; and 9 LCPO2000 broadband OBS from INSU, which are based on the "L-CHEAPO" instrument (Low-Cost Hardware for Earth Applications and Physical Oceanography) developed at the Scripps Institution of Oceanography (SIO).

We report on, and compare, the performance of seismometers and hydrophones from the two involved instrument pools, the German DEPAS and the French Parc Sismomètre Fond de Mer of INSU. This is the first side-by-side comparison of instruments from the German and French community OBS pools.

Data from the RHUM-RUM ocean bottom stations (and island stations) will be made freely available at the end of 2017 (Barruol et al., 2011).

This paper reviews the functioning of the OBS network and documents issues encountered in data collection, quality control, and processing. We review the experiment layout in Sect. 2.1, and the two types of OBS employed in Sect. 2.2. The performance of the stations is described in Sect. 3, with a focus on noise levels in Sect. 3.3. Possible reasons for the surprisingly different noise levels are discussed in Sect. 4.

Table 1. Data return in RHUM-RUM experiment.

Data return:	# of stations
Data return on all four channels throughout the entire deployment:	27
Data return on all four channels for only part of the deployment:	18
Only hydrophone data throughout the entire deployment:	1
Only hydrophone data for only part of the deployment:	7
No data returned:	4
Total number of stations deployed:	57
Data days recorded:	
Data days (hydrophones):	18 735
Data days (seismometers):	15 941
Deployment days:	19 751
Percent data recovery (hydrophones):	94 %
Percent data recovery (seismometers):	80 %

Appendix A contains a detailed description of the seismometer instrument responses, Appendix B describes an experiment to estimate clock drift rates and Appendix C contains a station-by-station list of noise levels in three period bands.

2 Experiment setup and instrumentation

2.1 The OBS network

For an overview of the whole network see Fig. 1. The oceanic component of the RHUM-RUM experiment consisted of 57 broadband ocean bottom seismometers deployed over an area of 2000 km × 2000 km from September 2012 to November 2013. The OBS clustered relatively densely around the island of La Réunion, out to distances of 400–500 km, including the vicinity of Mauritius (Fig. 1). This relative dense coverage was extended eastward to the Central Indian Ridge, in order to investigate hypothesized asthenospheric flow from hotspot to ridge (Morgan, 1978; Dyment et al., 2007). The seismicity in the reliably active South Sandwich subduction zone generates body-wave paths which sample the mantle beneath La Réunion at greater depths. Sampling with opposite azimuth is provided by earthquakes in the subduction zones of the south west Pacific, especially since the OBS network is augmented by RHUM-RUM land stations on Madagascar, and on the Îles Éparses in the Mozambique Channel. A linear, less dense arrangement of OBS followed the strike of the Central Indian and Southwest Indian ridges to the east and south, at 800–1200 km distance from the hotspot. Waves originating from earthquakes in the Alpine-Himalayan orogens and recorded at these stations again sample deeper levels of the mantle beneath La Réunion, but are also used to study the mid-ocean ridges themselves. A dense sub-array

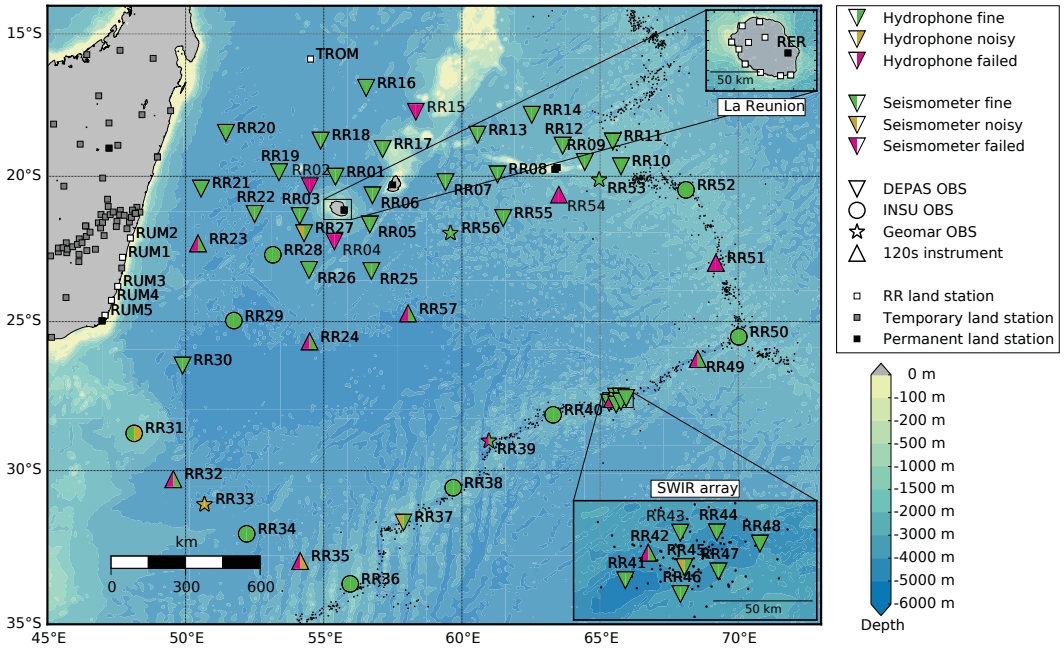

Figure 1. Overview map of the RHUM-RUM ocean bottom seismometer network. OBS are marked by large coloured symbols. Symbol shape marks the station type: DEPAS LOBSTER (inverted triangle), INSU LCPO2000 (circle), Geomar OBS (star). DEPAS instruments with malfunctioning 120 s instruments are marked as regular triangles. Two halves of the inner symbol indicate the functioning of the seismic sensors and hydrophones, respectively. Green indicates good performance; orange, high noise levels; red means the instrument failed to record. White squares indicate temporary land stations as part of the RHUM-RUM network YV, grey square indicate temporary land stations as part of the MACOMO (Wysession et al., 2012) and SELASOMA (Tilmann et al., 2012) projects, which were both installed between 2012 and 2014. Black squares indicate permanent GEOSCOPE stations. Small black dots mark earthquake hypocentres above magnitude 4 between 1981 and 2015, as published by the Preliminary Determination of Epicentres (PDE) bulletin of the US National Earthquake Information Center (NEIC). The seismicity is mainly concentrated on the oceanic ridges. Colour-shaded bathymetry is based on the global 30 arcsec merged bathymetry dataset by Becker et al. (2009), available at: http://topex.ucsd.edu/WWW_html/srtm30_plus.html.

of 8 OBS, referred to as the "SWIR Array", was deployed around an active seamount on the Southwest Indian Ridge in order to investigate the structure and seismicity of this ultra-slow spreading ridge. The sub-array had a footprint of about 70 km × 50 km and was located in segment 8 of the ridge, following the nomenclature of Cannat et al. (1999).

The OBS were deployed in October 2012 by the French research vessel *Marion Dufresne* and were recovered in October/November 2013 by the German research vessel *Meteor*. The instruments spent the intervening 13 months recording on the seafloor.

At each deployment site, the seafloor was surveyed with R/V *Marion Dufresne*'s multi-beam bathymeter and sediment echo sounder before dropping the OBS over board in a location deemed most suitable. The ship left immediately after deployment so that only deployment (and recovery) coordinates are known; no attempt was made to acoustically triangulate the landing positions of the OBS, with the notable exception of the 8 OBS in the densified SWIR Array. In general, OBS recovery positions were found to differ from their deployment positions by no more than a few hundred meters.

2.2 OBS models deployed

Here we give a brief overview of the hardware deployed (see Table 2) and the recording settings used, especially as they relate to the performance assessment of Sect. 3 (see Table 2 for an overview).

2.2.1 LOBSTER

The broadband OBS pool DEPAS (Deutscher Geräte-Pool für Amphibische Seismologie) of the German geophysical community consists of 80 instruments of the LOBSTER type ("Long-term OBS for Tsunami and Earthquake Research"). The OBS were developed in 2005, merging previous design experience mainly by Geomar Kiel (Flueh and Biolas, 1996), the University of Hamburg (Dahm et al., 2002), and the marine engineering firm K.U.M. (Umwelt- und Meerestechnik Kiel). K.U.M. was charged with building 80 LOBSTER units, which were funded by the German Research Foundation (DFG), the Federal Ministry of Education and Research (BMBF) and the Helmholtz Association of National Research Centres (HGF). The Alfred Wegener Institute Bremerhaven houses and maintains the instruments. For

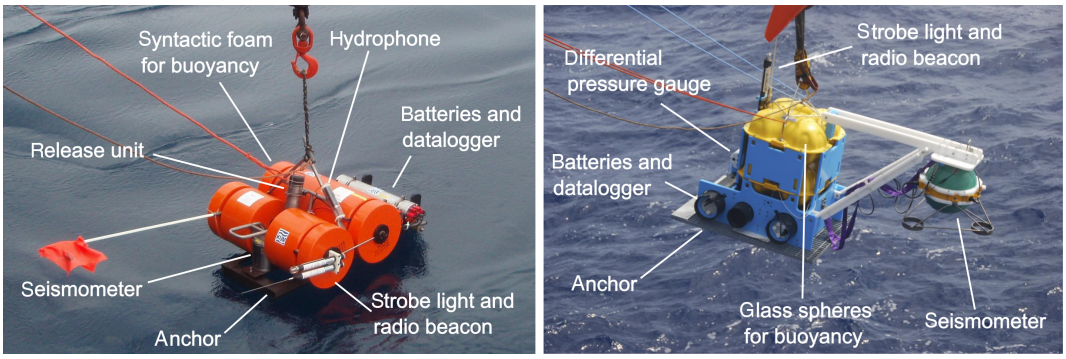

Figure 2. Broadband ocean-bottom seismometers, photographed seconds before deployment. Left panel: one of 48 LOBSTER-type instruments from the German DEPAS pool. The Güralp CMG-OBS40T sensor (corner period 60 s) is fitted in a vertical titanium pressure cylinder between two syntactic foam buoys and wedged against the steel anchor beneath it. Two horizontal titanium cylinders in the background contain the data recorder and the lithium batteries. The broadband hydrophone (corner period 100 s) is strapped to the A-shaped titanium frame that protrudes from the centre of the buoy assemblage. Right panel: one of 9 LCPO2000-BBOBS (Scripps-based) instruments from the French Parc de Sismomètre Fond de Mer pool at INSU. The Nanometrics Trillium sensor (corner period 240 s) is contained in the green sphere, which is dropped (i.e. mechanically separated) from the main frame one hour after arrival on the seabed. The differential pressure gauge is located in the white cylinder behind the frame. Both instruments are equipped with flags, strobe lights and radio beacons to facilitate recovery.

detailed information see http://www.awi.de/depas. The four OBS loaned to RHUM-RUM by Geomar Kiel are essentially identical to the DEPAS OBS.

The modular LOBSTER design (Fig. 2, left panel) is based on an open titanium frame that holds three titanium cylinders (containing the seismic sensor, data acquisition unit, and lithium batteries) and syntactic foam buoys that provide buoyancy for the ascent during recovery. A fourth titanium cylinder contains a mechanical release unit that locks the frame assemblage to a steel anchor until an acoustic release signal is received that initiates detachment from the anchor. The hydrophone is strapped to the frame, as are various recovery aides (a radio beacon, a flash, a flag, and a head buoy).

The titanium tube holding the seismic sensor is seated vertically between two syntactic foam units, and is wedged against the steel anchor by a steel plate, which acts as a lever that is pre-loaded by the mechanical release unit, thus ensuring good seismic coupling to the anchor. The integration of the seismometer into the frame makes the design very sturdy and reduces the number of failure points, but it also means that the seismometer is likely to record any tilt noise created by currents or pressure fluctuations acting on the frame. The orientation of the seismometer channels is fixed with respect to the frame, as it is shown in Fig. 3.

The seismic sensor in most DEPAS units is a three-component wideband Güralp CMG-OBS40T with a corner period of 60 s. The CMG-OBS40T is a lesser-known version of the CMG-40T with reduced power consumption, which is mounted in a gimbal system for usage in OBS. The gimbal system is activated three days after arrival on the seafloor to ensure proper levelling, since the instrument may land in a

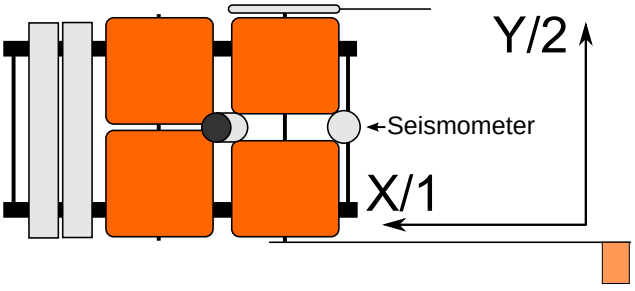

Figure 3. Sketch of a LOBSTER frame with the orientation of the horizontal seismometer channels. The X channel is oriented along the long axis of the LOBSTER, the Y channel 90° clock-wise of it. Positive values in the seismogram correspond to movement in the direction of the arrow. For the vertical (Z) channel, positive values correspond to upward movement. In the RESIF data archive, the X channel is stored as BH1, the Y channel as BH2 and the Z channel as BHZ.

tilted position) and then once every 21 days since the seafloor may settle over time.

The seismometer is sold in versions with different upper corner periods (10, 30, 60 s). All are mechanically identical, but use different feedback mechanisms to control the flat part of the response curve. The 60 s version is used by DEPAS and other OBS pools in Europe (e.g. IDL, Lisbon). Nine out of 48 instruments used in RHUM-RUM featured a prototype, broadband sensor design (corner period of 120 s). All of these nine units failed to level under deep-sea conditions, and repeated, unsuccessful levelling attempts drained the batteries prematurely (see Sect. 3.1).

The DEPAS units were additionally equipped with broadband hydrophones of type HTI-01 and HTI-04-PCA/ULF

Table 2. Comparison of German (DEPAS) and French (INSU-IPGP) OBS types.

Pool	DEPAS	INSU-IPGP
Manufacturer	K.U.M., Kiel	Scripps/INSU-IPGP
OBS type	LOBSTER	LCPO2000-BBOBS
Weight (water/air)	30/400 kg	25/350 kg
Assembly time	30 min (2 persons)	2 h (2 persons)
Transport options	12 in a 20′ container	8 in a 20′ container
Buoyancy	Syntactic foam	Glass spheres
Instrument casing	Titanium	Aluminium
Seismometer	CMG-OBS40T (60/120 s)	Trillium 240OBS (240 s)
Placement	integrated into frame	in external probe
Power consumption	100 mW (seism.) 520 mW (recorder)	700 mW (seism.) 600 mW (recorder)

manufactured by HighTechInc (corner period 100 s), which usually worked very reliably as long as power was available.

The deepest RHUM-RUM OBS was deployed at 5400 m depth (Table 3), and the standard DEPAS OBS is certified to 6000 m water depth. Two battery tubes can be fitted with up to 180 lithium cells, sufficient for up to 15 months of recording using the settings described below. RHUM-RUM instruments were equipped to record for 13 months at sampling rates of 50 Hz. Eight of the 48 available DEPAS units were of a deep-diving variant certified to 7300 m depth, which has only one battery tube and therefore holds fewer batteries. Most of these instruments were deployed in the SWIR sub-array and typically recorded for 8–9 months at a sampling rate of 100 Hz (higher rate in order to investigate local seismicity). The clocks are supposed to continue running even after the voltage has dropped below the level required for data recording, in order to enable estimates of clock drift even if OBS retrieval is delayed.

2.2.2 The Scripps OBS instrument, INSU instrument pool

The INSU instruments (Fig. 2, right panel) are of the LCPO2000-BBOBS type, which is based on the Scripps Institution of Oceanography (SIO) "L-CHEAPO" design. Three of the instruments were manufactured at SIO and the other six at the INSU-IPGP OBS facility. The data recorder, batteries and release unit are protected in aluminium cylinders. The seismic sensor sits in an aluminium sphere. Buoyancy for recovery is created by hollow glass spheres.

All instruments were equipped with Nanometrics Trillium-240 seismometers with a corner period of 240 s and a differential pressure gauge with a passband between 0.002 to 30 Hz.

The INSU instruments check their level every hour. This caused an electronic spike of approximately 600 counts on the seismometer channels (see Sect. 3). This same spike exists in the 2006–2007 PLUME data set using SIO BBOBS (Laske et al., 2009), although we found no published mention of it. The problem has not been explicitly solved, but the SIO BBOBSs were reprogrammed after the PLUME experiment to only check level once a week after the initial levelling cycle and the INSU BBOBSs are currently being reprogrammed to do the same. Work has been done to remove the hourly spike in the PLUME data (G. Laske, personal communication, 2014) and is being repeated for the RHUM-RUM data: it would be good to publish the correction algorithms, because these instruments probably still have this spike once per week.

The INSU instruments use a differential pressure gauge (DPGs, Cox et al., 1984) rather than a hydrophone. The DPG sits on the lower instrument frame close to the battery cylinder (Fig. 2).

2.3 Instrument responses

Instrument responses specify the transfer functions of seismometers and hydrophones (three seismogram channels and one hydrophone channel per station). The RESIF (RÉseau SIsmologique & géodésique Français) data centre serves this information in the format of StationXML or dataless SEED files.

To our knowledge, detailed meta-data information for DEPAS OBS has not been published elsewhere. Therefore, we added a detailed discussion of the instrument responses as an appendix to this paper (Sect. A). Figures 4 and 5 show the total responses of instruments and data loggers for hydrophones and seismometers. Figure 6 shows instrument-corrected waveforms. For all seismometer types, instrument correction results in the same P-waveform.

3 Network performance

All 57 OBS were recovered successfully and undamaged. Table 3 summarizes the state of health of all seismometers and hydrophones over the deployment period. For a graphical summary of network performance (see Fig. 7).

Deployments were staggered over four weeks, along the 15 000 km-long cruise track. Recovery took five weeks and proceeded in roughly the same order as deployment, so that all stations spent approximately 13 months on the sea floor. An early end of recording was anticipated for stations RR35, RR41, RR43–RR48, and RR51 because their single battery tube only accommodated batteries for 8–9 months. For other stations, premature end of recording reflects technical issues, as discussed below.

Following the definition of the Cascadia initiative (Sumy et al., 2015), the data recovery was 15 941 data days out of 19 751 deployment days or 80 % for the seismometers, and 18 735 data days or 94 % for the hydrophones (Table 1).

Table 3. Performance summary of the 57 RHUM-RUM OBS and hydrophones. The abbrevation "gz" in the status column refers to the "glitch" on the *Z* component of the INSU seismograms (see Sect. 3.1). Skew is the measured clock drift in s, i.e. the instrument time at recovery minus the GPS time at recovery ("NA" if unknown because clock stopped early). For DEPAS stations, the number of recording days can exceed the number of deployment days because recording was started on deck prior to deployment. In the comments column, "120 s inst." refers to the new DEPAS sensor type that failed to level, yielding no useful seismometer data; "Geomar" refers to an OBS from Geomar, similar to the DEPAS LOBSTER. Figure 7 summarizes the network's state of health over the deployment period of October 2012 to November 2013.

Station name	Latitude	Longitude	Depth [m]	Deployment date [UTC]	Recovery date [UTC]	End of record [UTC]	Install. time [days]	Record length [days]	s.r. [Hz]	Seismo status	Hydro status	Skew value	Notes
RR01	−20.0069	55.4230	4298	5 Oct 2012	6 Nov 2013	6 Nov 2013	397	397	50	good	good	0.67 s	
RR02	−20.3392	54.4984	4436	5 Oct 2012	6 Nov 2013	5 Oct 2012	396	0	50	failed	failed	NA	
RR03	−21.3732	54.1294	4340	5 Oct 2012	5 Nov 2013	5 Nov 2013	396	396	50	good	good	0.81 s	
RR04	−22.2553	55.3846	4168	5 Oct 2012	5 Nov 2013	7 Oct 2012	396	2	50	failed	failed	NA	
RR05	−21.6626	56.6676	4092	3 Oct 2012	5 Nov 2013	2 Nov 2013	398	395	50	good	good	0.93 s	
RR06	−20.6550	56.7639	4216	3 Oct 2012	7 Nov 2013	31 Oct 2013	399	393	50	good	good	NA	
RR07	−20.1945	59.4058	4370	29 Sep 2012	24 Oct 2013	24 Oct 2013	389	389	50	good	good	0.53 s	
RR08	−19.9259	61.2907	4190	29 Sep 2012	24 Oct 2013	24 Oct 2013	389	389	50	good	good	1.40 s	
RR09	−19.4924	64.4485	2976	30 Sep 2012	25 Oct 2013	25 Oct 2013	389	390	50	good	good	2.18 s	
RR10	−19.6437	65.7558	2310	30 Sep 2012	25 Oct 2013	25 Oct 2013	390	390	50	good	good	0.39 s	
RR11	−18.7784	65.4629	3941	1 Oct 2012	26 Oct 2013	26 Oct 2013	390	390	50	good	good	0.61 s	
RR12	−18.9255	63.6474	3185	1 Oct 2012	26 Oct 2013	26 Oct 2013	390	390	50	good	good	−0.11 s	
RR13	−18.5427	60.5635	4130	2 Oct 2012	27 Oct 2013	9 Oct 2013	390	372	50	good	good	NA	
RR14	−17.8448	62.5299	3420	1 Oct 2012	27 Oct 2013	27 Oct 2013	390	390	50	good	good	2.36 s	
RR15	−17.7402	58.3330	3959	2 Oct 2012	28 Oct 2013	4 Oct 2012	390	1	50	failed	failed	NA	
RR16	−16.8976	56.5335	4426	2 Oct 2012	28 Oct 2013	28 Oct 2013	391	391	50	good	good	1.61 s	
RR17	−19.0427	57.1322	2205	3 Oct 2012	23 Oct 2013	23 Oct 2013	385	385	50	good	good	1.82 s	
RR18	−18.7504	54.8878	4743	6 Oct 2012	29 Oct 2013	29 Oct 2013	388	388	50	good	good	0.36 s	
RR19	−19.8500	53.3805	4901	9 Oct 2012	30 Oct 2013	30 Oct 2013	385	386	50	good	good	1.67 s	
RR20	−18.4774	51.4600	4820	6 Oct 2012	30 Oct 2013	30 Oct 2013	389	389	50	good	good	0.41 s	
RR21	−20.4217	50.5599	4782	7 Oct 2012	31 Oct 2013	31 Oct 2013	389	389	50	good	good	0.27 s	
RR22	−21.3007	52.4994	4920	9 Oct 2012	1 Nov 2013	1 Nov 2013	387	387	50	good	good	0.89 s	
RR23	−22.3290	50.4487	4893	10 Oct 2012	31 Oct 2013	26 Aug 2013	386	320	50	failed	good	NA	120 s inst
RR24	−25.6805	54.4881	5074	22 Oct 2012	3 Nov 2013	8 Oct 2013	376	291	50	failed	good	NA	120 s inst
RR25	−23.2662	56.7249	4759	4 Oct 2012	4 Nov 2013	4 Nov 2013	396	396	50	good	good	0.43 s	
RR26	−23.2293	54.4698	4259	4 Oct 2012	2 Nov 2013	2 Nov 2013	393	393	50	good	good	0.63 s	
RR27	−21.9657	54.2889	4277	5 Oct 2012	5 Nov 2013	19 Jul 2013	396	286	50	noisy	good	NA	
RR28	−22.7152	53.1595	4540	10 Oct 2012	12 Nov 2013	12 Nov 2013	398	397	62.5	good (gZ)	good	3.10 s	INSU
RR29	−24.9657	51.7488	4825	11 Oct 2012	13 Nov 2013	13 Nov 2013	398	397	62.5	good (gZ)	good	3.37 s	INSU
RR30	−26.4861	49.8917	5140	11 Oct 2012	14 Nov 2013	8 Oct 2013	398	361	50	good	good	NA	
RR31	−28.7648	48.1394	2710	12 Oct 2012	15 Nov 2013	15 Nov 2013	398	398	62.5	good (gZ)	noisy	−0.83 s	INSU
RR32	−30.2903	49.5555	4670	12 Oct 2012	15 Nov 2013	6 Nov 2013	398	358	50	failed	good	NA	120 s inst
RR33	−31.1170	50.6835	4904	13 Oct 2012	16 Nov 2013	19 Sep 2013	399	341	50	noisy	noisy	NA	Geomar
RR34	−32.0783	52.2113	4260	13 Oct 2012	16 Nov 2013	16 Nov 2013	399	398	62.5	good (gZ)	good	−1.29 s	INSU
RR35	−32.9694	54.1473	4214	13 Oct 2012	17 Nov 2013	27 May 2013	399	225	50	failed	noisy	NA	120 s inst
RR36	−33.7018	55.9578	3560	14 Oct 2012	17 Nov 2013	17 Nov 2013	399	398	62.5	good (gZ)	good	3.06 s	INSU
RR37	−31.7010	57.8876	4036	14 Oct 2012	18 Nov 2013	19 Oct 2013	399	369	50	noisy	good	NA	
RR38	−30.5650	59.6858	4540	15 Oct 2012	19 Nov 2013	19 Nov 2013	399	399	62.5	good (gZ)	good	−0.06 s	INSU
RR39	−29.0165	60.9755	4700	15 Oct 2012	19 Nov 2013	19 Nov 2013	400	400	50	failed	noisy	NA	Geomar
RR40	−28.1461	63.3020	4750	16 Oct 2012	20 Nov 2013	20 Nov 2013	400	399	62.5	good (gZ)	good	0.19 s	INSU
RR41	−27.7330	65.3344	5430	16 Oct 2012	20 Nov 2013	17 Jun 2013	400	244	100	good	good	NA	
RR42	−27.6192	65.4376	4776	16 Oct 2012	21 Nov 2013	10 Aug 2013	400	298	50	failed	good	NA	120 s inst
RR43	−27.5338	65.5826	4264	16 Oct 2012	21 Nov 2013	15 Jun 2013	401	241	100	good	good	NA	
RR44	−27.5324	65.7480	4548	16 Oct 2012	22 Nov 2013	3 Jun 2013	401	229	100	good	good	NA	
RR45	−27.6581	65.6019	2822	16 Oct 2012	21 Nov 2013	4 Jun 2013	400	138	100	noisy	good	NA	

Table 3. Continued.

Station name	Latitude	Longitude	Depth [m]	Deployment date [UTC]	Recovery date [UTC]	End of record [UTC]	Install. time [days]	Record length [days]	s.r. [Hz]	Seismo status	Hydro status	Skew value	Notes
RR46	−27.7909	65.5835	3640	16 Oct 2012	21 Nov 2013	26 May 2013	400	221	100	good	good	NA	
RR47	−27.6958	65.7553	4582	16 Oct 2012	21 Nov 2013	22 Jun 2013	400	248	100	good	good	NA	
RR48	−27.5792	65.9430	4830	16 Oct 2012	22 Nov 2013	10 Jun 2013	401	237	100	good	good	NA	
RR49	−26.2742	68.5354	4444	17 Oct 2012	23 Nov 2013	6 Nov 2013	401	384	50	failed	good	NA	120 s inst
RR50	−25.5181	70.0222	4100	18 Oct 2012	23 Nov 2013	23 Nov 2013	401	400	62.5	good (gZ)	good	1.74 s	INSU
RR51	−22.9989	69.1911	3463	18 Oct 2012	24 Nov 2013	3 Jan 2013	401	76	50	failed	failed	NA	120 s inst
RR52	−20.4722	68.1094	2880	19 Oct 2012	25 Nov 2013	25 Nov 2013	401	401	62.5	good (gZ)	good	0.97 s	INSU
RR53	−20.1213	64.9664	2940	20 Oct 2012	28 Nov 2013	30 Oct 2013	403	375	50	good	good	NA	Geomar
RR54	−20.6424	63.5082	2499	20 Oct 2012	28 Nov 2013	21 Oct 2013	404	365	50	failed	good	NA	120 s inst
RR55	−21.4417	61.4959	4462	20 Oct 2012	28 Nov 2013	8 Nov 2013	404	383	50	good	good	NA	
RR56	−21.9694	59.5853	4230	21 Oct 2012	29 Nov 2013	29 Jun 2013	404	251	50	good	good	NA	Geomar
RR57	−24.7264	58.0496	5200	21 Oct 2012	3 Nov 2013	31 Oct 2013	378	374	50	failed	good	1.28 s	120 s inst

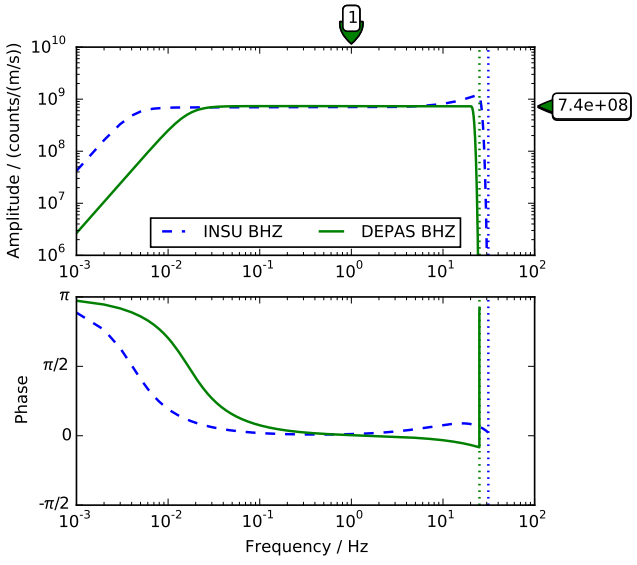

Figure 4. Bode plot of the total instrument responses $G(f)$ as defined in Eq. (A2) of vertical seismometer components, for a DEPAS Güralp CMG-OBS40T seismometer (solid green, station RR26), and for an INSU Trillium-240 (dashed blue, RR28). The corner period is 60 s for DEPAS instruments and 240 s for INSU instruments, which is evident from the amplitude responses. Horizontal channel responses of DEPAS instruments are identical to vertical responses, apart from the channel-specific gain, which varies by a few percent. The horizontal gain of INSU sensors is 1.6×10^8 counts$(\mathrm{m\,s^1})^{-1}$ compared to of 7.0×10^8 counts$(\mathrm{m\,s^1})^{-1}$ for the vertical channel. The upper frequency limits (dotted lines) are given by the Nyquist frequencies ($1/2 \times 50$ Hz for RR26 and $1/2 \times 62.5$ Hz for RR28).

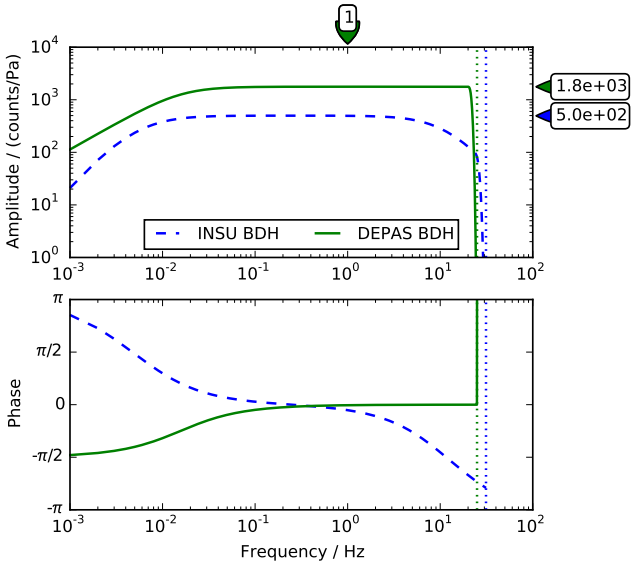

Figure 5. Bode plot of the total instrument responses $G(f)$ as defined in Eq. (A2) of a DEPAS HighTechInc HTI-PCA04/ULF hydrophone (solid green, station RR26), and of an INSU differential pressure gauge (dashed blue, RR28). The nominal corner period is 100 s for DEPAS instruments and 500 s for INSU instruments. Dotted lines mark the Nyquist frequencies (see above).

3.1 Instrument failures

Three out of 48 DEPAS stations (RR02, RR04, RR15) delivered neither seismometer nor hydrophone data because their data loggers failed (reason unclear). The seismometers in nine DEPAS stations (RR23, RR24, RR32, RR35, RR42, RR49, RR51, RR54, RR57) featured a redesigned sensor/casing package with broader band CMG-OBS40T sensors (120 s), which had previously not been deployed in the deep sea. The levelling mechanisms failed (remained stuck) in all nine stations, for reasons that are still under investigation. Automatic, prolonged attempts to level the sensors drained their batteries prematurely so that the functioning hydrophones also ran out of power 8–9 months into the experiment. DEPAS seismometers RR27 and RR45 recorded, but at high noise levels (reason under investigation). The hydrophones of these stations worked normally. The seismometer in one of the four Geomar stations failed (RR39), and noise levels at Geomar station RR33 are unusually high, al-

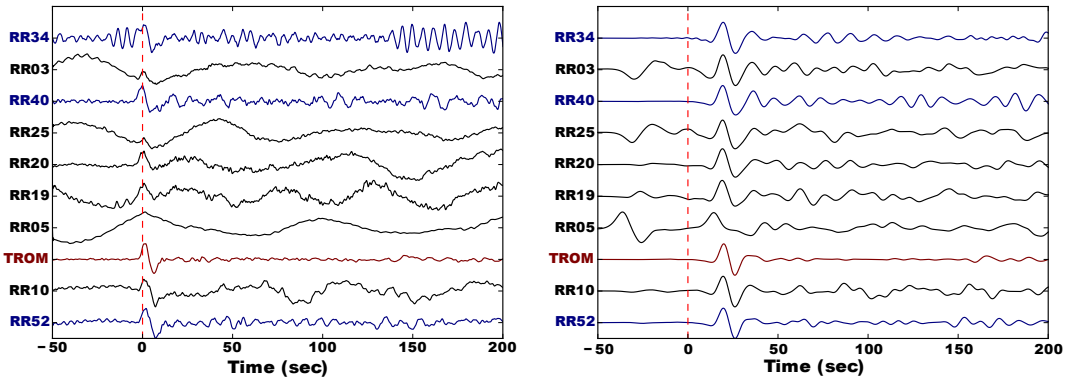

Figure 6. Comparison of broadband (left panel) and bandpass-filtered seismograms for six DEPAS OBS (black), three INSU OBS (RR34, RR40, RR52, blue) and an island station (TROM on Île Tromelin, red) in the northern part of the OBS network (see Fig. 1). All seismograms have been instrument-corrected to displacement, filtered between 1/60 and 3 Hz (the nominal corner frequencies of the least broadband sensor type, the DEPAS OBS) in order to facilitate visual comparison. The waveforms on the right have been bandpass-filtered using a Gabor filter as described in Sigloch (2008, p. 100) with a centre frequency of 1/15 Hz. Waveforms are amplitude-normalized and plotted relative to the theoretical arrival time of a P-wave from a magnitude 6.6 earthquake on 20 April 2013 in Sichuan, China (71° distance, see GEOFON, 2013). This shows that the instrument response has been determined correctly and that even the relatively noisy DEPAS recordings can be used for purposes like waveform tomography. The band-pass filter strongly enhances the P-wave, compared to the wideband traces, where it is lost in the long period noise for most DEPAS stations.

though this might not be due to the sensor. The hydrophones in RR33 and RR39 measured, but at a high noise level.

The 9 INSU stations (RR28, RR29, RR31, RR34, RR36, RR38, RR40, RR50, RR52) were affected by a bug in the data logger software that activated the level-sensing circuitry every 3620 s (roughly every hour). Each such event caused a "glitch" in the seismograms of roughly 1200 s duration, i.e. a characteristic, complex pulse shape, that is very similar but not identical across events. Pulse amplitudes are between 500–800 counts, corresponding to 1.5 µm ground displacement after instrument correction and filtering between 20 and 500 s period. This artefact is rarely visible on horizontal components where noise levels are much higher in this period band, but it exceeds noise amplitudes on the vertical channels by 15 dB. Figure 8 shows that the glitch amplitude is comparable to body wave arrivals of intermediate-size, teleseismic earthquakes, here a M6.6 earthquake at 71° distance. Efforts are under way to suppress this artefact by matched filtering.

The differential pressure gauge in INSU station RR31 had high artefacts roughly every 9000 s. Seismic signals are visible in between, but may be difficult to use. For station RR38, gaps in the data had to be fixed. Although this was carefully done, it is possible that artefacts were introduced.

3.2 Estimation of clock error

The internal clocks of the data recorders are affected by drifts on the order of one second per year. Over 13 months of autonomous recording, drift of this magnitude is non-negligible for certain applications, such as body-wave tomography. Prior to deployment, each recorder clock was synchronized to GPS, and upon recovery it was compared to GPS time again, yielding the clock drift or "skew". Assuming that the skew accumulated linearly over the deployment period, the clock error can be corrected for any moment in time. Previous studies (Hannemann et al., 2014; Scholz, 2014) show that linearity is a good first order approximation for the clocks used in the DEPAS instruments. For the LCPO2000 instruments used in the INSU pool, Gouedard et al. (2014) found that drift rates can vary over the course of days. We assume that this effect is cancelling out for longer deployments, therefore RHUM-RUM data at the RESIF data centre are linearly corrected for skew, where available.

Unfortunately a significant number of DEPAS clocks stopped before recovery, so that the skew could not be measured (entries "NA" in Table 3). Clock shutdown was not anticipated even if batteries became weak. At a critical voltage level of 6.0 V (down from 13.0 V), the recorder was programmed to switch off seismometer and hydrophone, allowing its low-consuming clock to continue for several months. The Lithium batteries for long-term deployments have a faster current drop than the alkali batteries for normal deployments, which caused a problem for multiple stations. Superimposed on a gradual voltage decline, the log files show brief, steep voltage drops associated with levelling events every 21 days. Towards the end of the recording period, this led to uncontrolled shutdown of some recorders and clocks, presumably when a drop below critical voltage occurred too suddenly.

Using cross-correlation of ambient noise, Sens-Schönfelder (2008) presented a method to determine the relative clock error between two seismometers a posteriori, which Hannemann et al. (2014) successfully applied to OBS data. Likewise, Scholz (2014) succeeded in estimating

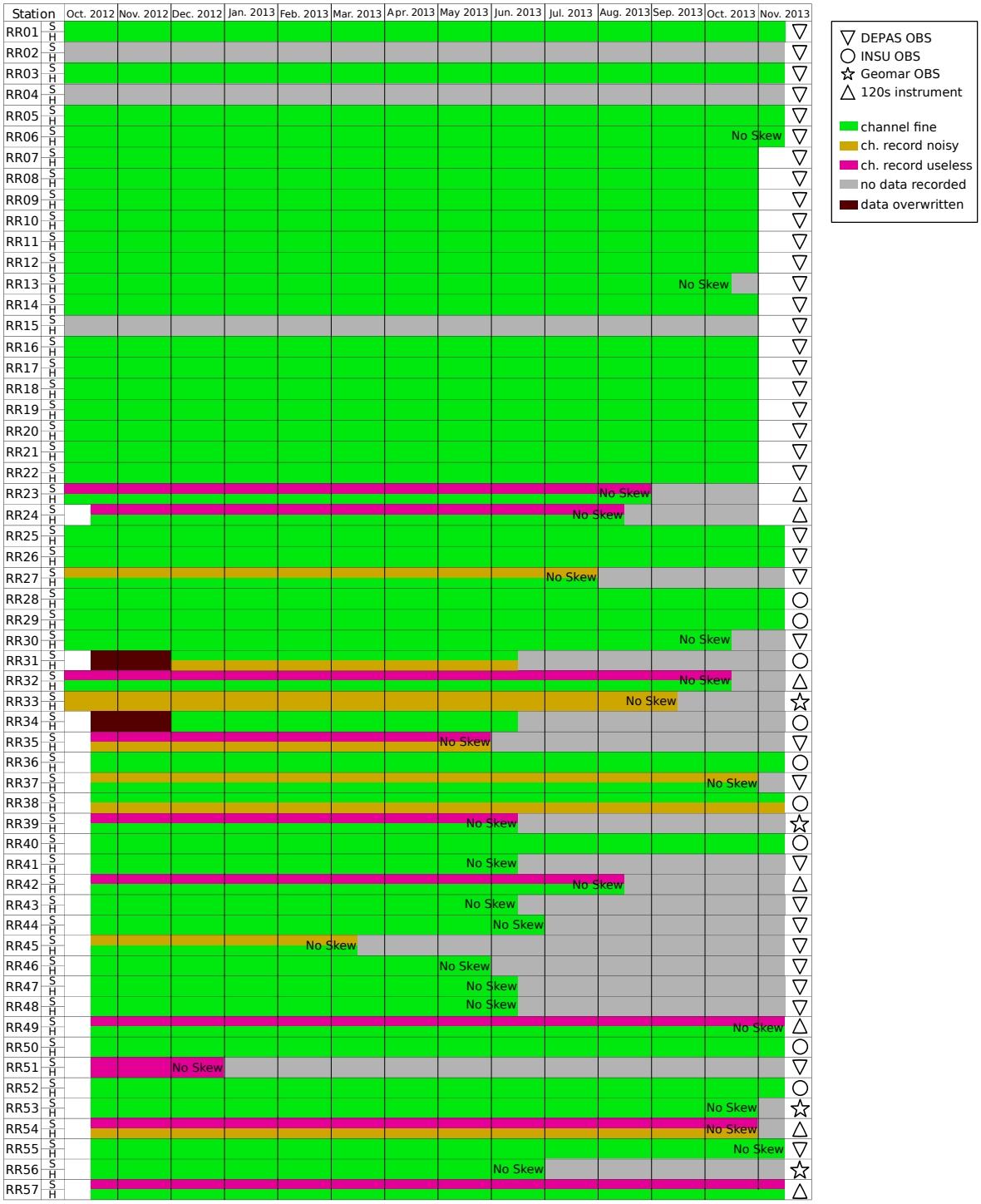

Figure 7. Data availability and quality for all RHUM-RHUM ocean-bottom stations. Green indicates availability of good data. Yellow indicates availability of abnormally noisy data, where earthquakes are visible, but artefacts are so strong, that noise correlation or other advanced analyses will probably fail. Red indicates that the seismometer ("S" in first column) or hydrophone/differential pressure gauge ("H") recorded data that is completely useless for seismological purposes. These time traces will still be archived at RESIF and may be useful for analysis of error sources. Grey shading indicates time intervals when battery power had run out prior to recovery, or where the data logger failed (RR02, RR04, RR15) and no data was recorded at all. Dark red shading indicates time intervals of missing data for INSU stations RR31 and RR34 (overwritten due to erroneous reset of data logger). Station symbols in the last column follow Fig. 1. Inverted Triangles: regular DEPAS LOBSTER (seismometer 60 s corner period, 50 Hz sampling rate); stars: Geomar LOBSTER (60 s, 50 Hz); regular triangles: newer DEPAS LOBSTER (120 s corner period, all seismometers failed); circles: INSU/Scripps instrument (240 s, 62.5 Hz).

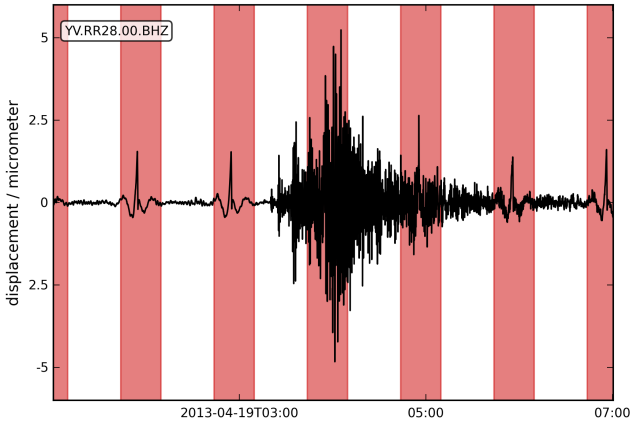

Figure 8. A M6.6 earthquake at 71° distance recorded on the vertical component of INSU OBS RR28. The seismogram has been instrument-corrected to ground displacement and passband-filtered at 20 to 500 s. One red plus one white stripe span 3620 s, slightly more than one hour. The seismogram shows one "glitch" per red shaded interval, i.e. nearly hourly, pulse-like artefacts caused by unintended activation of the sensor levelling mechanism in INSU stations. One glitch is hidden by the surface wave train. The earthquake is the same as in Fig. 6 (66° distance, see GEOFON, 2013).

clock drift for the SWIR sub-array of the RHUM-RUM network (RR42-RR48, inter-station distances of 30–40 km). His results suggest that indeed clock errors accumulated linearly over the installation period. For the remainder of the RHUM-RUM network, inter-station distances were unfortunately found to be too large (> 150 km) to apply this ambient noise method, especially given the high self-noise level of the DEPAS OBS packages.

In an attempt to estimate the clock drift of these 11, otherwise well-functioning OBS a posteriori, we did a dry run of several recorders in the DEPAS lab with batteries and seismometers attached for over a month. Afterwards, we compared the value of the internal clock with GPS time. These experiments reproduced the sign of the clock error (clocks generally ran too slow) but probably not their values, at least not to an accuracy that would be useful in practice. The likely reason is that we did not simulate the low water temperatures on the seafloor. The experiment is described in detail in Appendix B.

3.3 Noise levels

Noise levels can be characterized by Probabilistic Power Spectral Density distributions (PPSDs, McNamara and Buland, 2004) for each of the four sensor components. We obtain PPSDs by computing power spectra on hour-long broadband time series, and by stacking the hourly results over the recording period. Figure 9 shows PPSDs for DEPAS station RR26 (depth 4259 m) and for INSU station RR28 (depth 4540 m), which were deployed at 150 km distance between each other.

We created a poster of PPSDs for all 57 stations and all 4 channels, which is published as a Supplement to this article and shows that the relative noise differences of Fig. 9 are characteristic for INSU versus DEPAS stations more generally.

3.3.1 Vertical seismometer channels

The seismometer spectra are rather similar at short periods but increasingly divergent at periods longer than 5 s. The vertical channel (BHZ) of the INSU instrument has its low-noise notch at 10–30 s period and stays well below the bounds of the (terrestrial) New High Noise Model (Peterson, 1993), to periods longer than 200 s. The BHZ channel of the DEPAS instrument has its low-noise notch around 10–15 s; at longer periods, the noise rapidly increases, rising well above the Peterson High Noise Model.

At 40 s period, the noise level on the BHZ channel is around −125 dB for DEPAS instruments and −155 dB for INSU instruments. These values are before correction for tilt or sea floor compliance (Crawford and Webb, 2000). At periods longer than 20 s, noise levels on BHZ show little amplitude variation over the deployment period, with a variance of roughly 10 dB at most stations (Fig. 9).

3.3.2 Horizontal seismometer channel

Noise on the horizontal seismometer channels is much higher than on the vertical for both instrument types. Horizontal components show mean noise levels between −100 and −115 dB for DEPAS OBS, and around −135 dB for INSU instruments (at 40 s period). The variance is on the order of 20 dB and shows clear seasonal variations (Fig. 10).

Tilting of the instrument, e.g. caused by underwater currents shaking the OBS frame (Duennebier et al., 1981; Trehu, 1985; Webb, 1998) affects the horizontal channels much more than the vertical component, so the higher horizontal noise level is expected.

3.3.3 Hydrophone channel

The spectra of DEPAS hydrophones and INSU differential pressure gauges are rather similar across the entire frequency range, both in general shape and in absolute decibel levels (see Figs. 9, C1, C2 and C3). This is in marked contrast to the large differences in seismometer noise levels between DEPAS and INSU instruments, and again points to a tilt origin or self-noise for the DEPAS seismometer noise, since tilt would hardly affect hydrophone records.

The pressure noise at DEPAS hydrophone RR26 is even slightly lower than at the near-by INSU RR28 (Fig. 9). In general, hydrophone noise levels are approximately 5 dB lower on DEPAS stations than on INSU stations in the period range of 12–40 s (see Fig. C2 in the appendix). This is true for the DEPAS hydrophones in general, with the exception of only a few noisy outliers that had individual problems. The

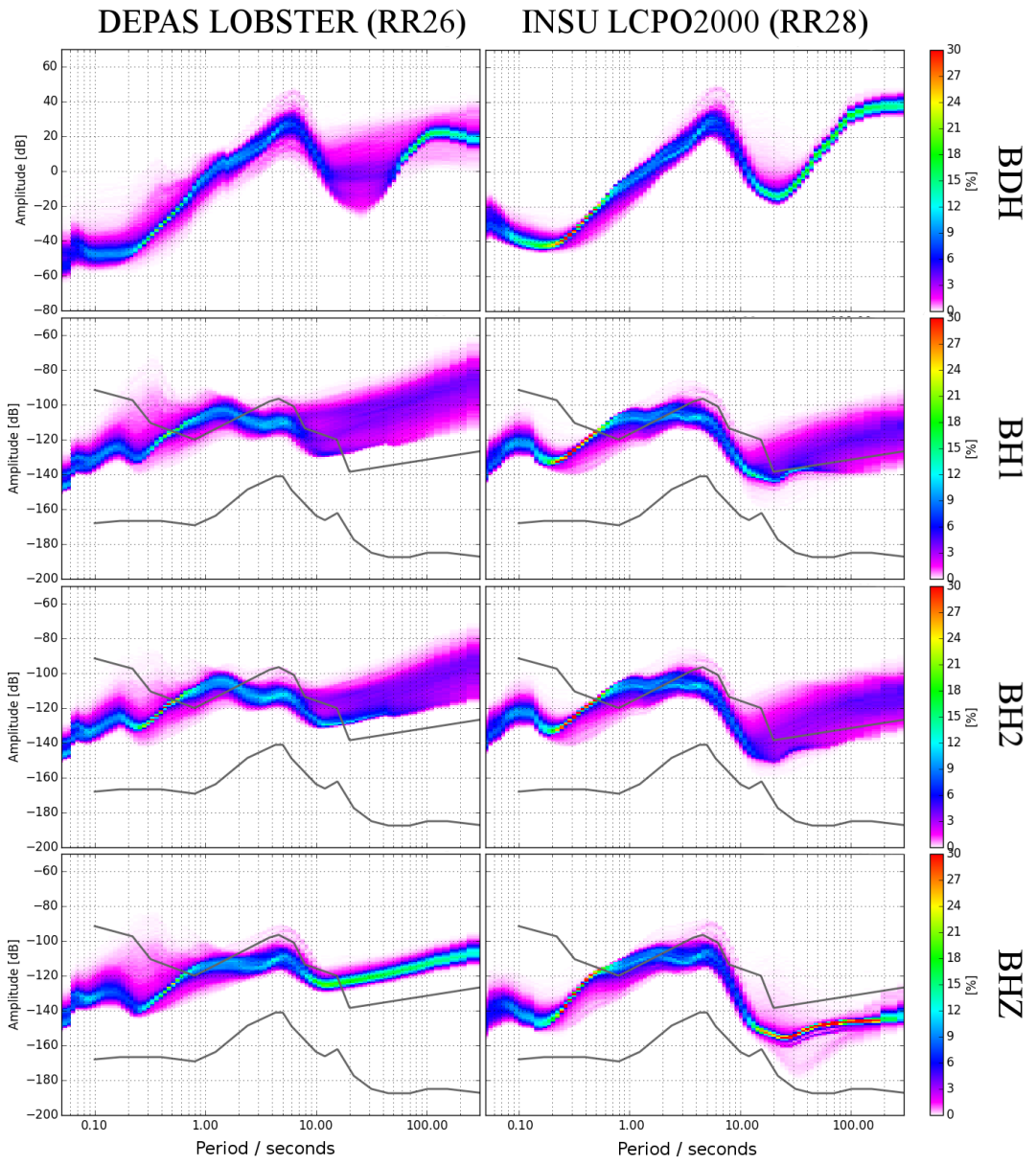

Figure 9. Probabilistic power spectral densities (PPSDs) for a DEPAS station (RR26, left column panels) and an INSU station (RR28, right column panels). PPSDs are composed of hour-long power spectra stacked over the entire deployment interval. Colour marks the frequency of occurrence of different noise levels, where purple indicates relatively rare, and red relatively frequent (McNamara and Buland, 2004). Black curves mark the upper and lower bounds of the New High and Low Noise Model of Peterson (1993). The two instruments were installed within 150 km of each other, in an abyssal plain 300 km south-west of La Réunion island (cf. Fig. 1). At periods longer than 5 s, the INSU seismometers are much quieter than the DEPAS instrument (see Sect. 4). By contrast, the pressure channel BDH of the two models (hydrophone for DEPAS, differential pressure gauge for INSU) shows very similar noise levels. A poster with PPSDs for all stations is available on ResearchGate (Stähler et al., 2015) and as an Supplement to this paper.

overall lower noise level can probably be explained by completely different instrument types (hydrophones on DEPAS versus differential pressure gauges on INSU stations).

3.4 Temporal noise variations

We expect two sources for temporal noise variations: (1) varying wave heights due to storm activity, which affects mostly the microseismic noise band. (2) Water current-induced tilt, which creates long period noise.

Figure 10 shows the temporal evolution of noise levels between October 2012 and October 2013 at DEPAS station RR01 near La Réunion (depth 4298 m), between 2 and 60 s). In the secondary microseismic noise band (2–10 s period), peak noise intervals coincide with cyclone passages during southern summer (blue frames). Cyclones are tropical storms, the Indian Ocean equivalent of hurricanes and typhoons. Their correlation to microseismic noise is most pronounced on the BHZ component. In fact, Davy et al. (2014) were able to track the path of a cyclone across the RHUM-RUM network using recordings of secondary microseismic noise only.

By contrast, peak noise episodes in the 20–60 s band show no clear correlation with cyclone passages. Rather, the highest levels occur during southern winter (March to September), out of cyclone season. Seasonal variations in deep-sea currents might explain tilt noise at these lower frequencies. The HYCOM-based global ocean circulation model (`GLBa0.08/expt_90.9`) (Cummings, 2005) does predict more episodes of strong currents at RR01 during southern autumn, (Fig. 10 bottom), but its absolute velocity values would appear low for effectively shaking an OBS. However, global ocean circulation models for this region have very poor resolution in the bottom layer, so that true bottom currents may be different. A recent measurement of current profiles at 23° S, 48° E (Ponsoni et al., 2015) suggests that bottom velocities generally do not exceed a few cm per second in the region (L. Ponsoni, personal communication, 2015). Unfortunately, the nearest RHUM-RUM station, (RR23) failed to deliver seismograms for comparison.

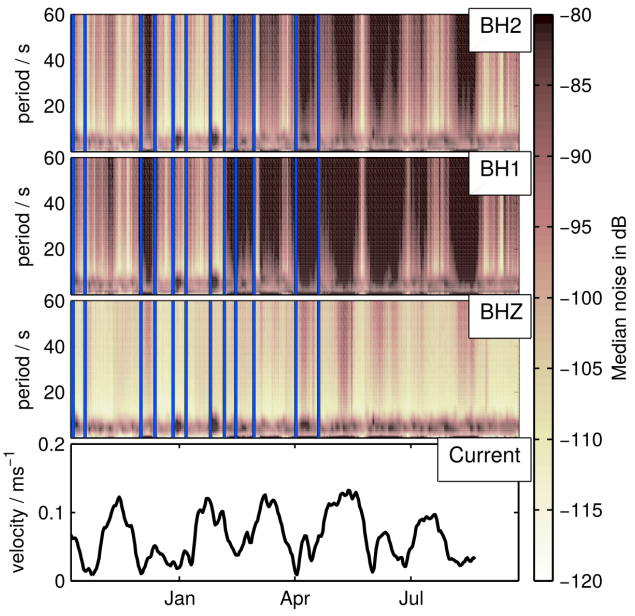

Figure 10. Seasonal changes in the noise levels on OBS RR01 near La Réunion. Spectrograms of noise on the three seismometer components, where noise is plotted as the median of daily probabilistic power spectral densities. Blue boxes mark episodes of cyclone activity, which correlates well with peak noise episodes in the microseismic band (periods around 10 s), especially on the BHZ component. At periods longer than 20 s, seismic noise peaks occur preferentially in southern autumn (February–June), most evident on the horizontal components. The global ocean circulation model HYCOM GLBa0.08/expt_90.9, running from 3 January 2011 to 20 August 2013 predicts more intervals of strong ocean-bottom currents for southern autumn (bottom panel) – qualitatively consistent with the hypothesis that ocean bottom currents cause long-period OBS noise by tilting the seismic sensors.

4 Discussion of the different noise levels

The relative stronger overall noise on the DEPAS instrument affects the usability of the OBS for waveform tomography and analysis of long-period waveforms. Hence its causes are of interest to future users of the pool and for instrument developers. We discuss four potential differences between the two instrument types:

The gimbal system: if the gimbal system were not stable enough, it could cause additional noise on all components. This hypothesis cannot be proven or falsified, since the CMG-OBS40T cannot be tested outside its gimbal. Experience shows that this would rather cause high-frequency noise.

The data logger: the data loggers of the DEPAS and the INSU OBS could have different self-noise levels. Again, this cannot be tested, since we have no data from other loggers available. But similar to the gimbal system, this would rather affect the high-frequency end of the spectrum, which is similar for both types.

OBS tilt: the integration of the seismometer into the OBS frame makes the DEPAS instruments more susceptible to current-induced tilt. Seasonal variations on the noise level of the horizontal channels can be seen in Fig. 10 and in the cloudy look of the PPSDs beyond 10 s in Fig. 9. However, tilt noise should affect horizontal channels much more strongly than vertical ones, which is indeed the case for the INSU instruments. For the DEPAS instruments, the vertical noise is too high to be explained by tilt alone.

Seismometer self noise: the CMG-OBS40T is a 60s wideband instrument, based on the 10 s CMG-40T. While the self noise of the latter is below the New Low Noise Model (NLNM) for periods shorter than 10s, onshore experiments with one of the CMG-OBS40Ts showed self noise of −140 dB at 10 s period, which is far above the NLNM. This strongly suggests that the reduced power consumption of the OBS40T comes at the price of a significantly increased self-noise level. High self-noise probably explains the larger part of the excessive noise on the vertical channel in our experiment.

To summarize, we expect the high noise level of the DEPAS instruments to be caused by a combination of tilt and instrument self noise, where the former dominates the noise on the horizontal channels and the latter the noise on the vertical channel. The fact that the variability of noise on the horizontal channels is comparable between the two instrument types suggests that the susceptibility to currents is similar, albeit slightly higher on the DEPAS instrument package. The usage of a compact wideband sensor in the LOBSTER instruments has the advantage of a much lower power consumption, at the price of a strongly increased noise level beyond 10 s.

More detailed analysis of the effect of sensor integration would require usage of a more broadband sensor in the DEPAS instrument package.

5 Conclusions

From October 2012 to November 2013, the RHUM-RUM experiment deployed and successfully recovered 48 German DEPAS and 9 French INSU broadband ocean-bottom seismometers around La Réunion, western Indian Ocean, making this the largest deployment of either instrument type, and the only joint experiment. Overall network performance was very satisfactory, but a number of technical issues have been described here, including blocked levelling mechanisms, data logger malfunctioning, and loss of clock synchronization.

For the first time, we publish instrument response information on the DEPAS OBS, which allows to calculate the true ground displacement in a wide frequency range.

This shows that at periods longer than 10 s, the INSU OBS are much quieter than the DEPAS instruments, on all three seismometer components. No such difference in data quality exists for the hydrophones and differential pressure gauges, which both worked extremely reliably. The increased long-period noise on the DEPAS seismometers can be explained by the surprisingly high instrument self-noise on the all channels of the Güralp CMG-OBS40T sensors and partially by a higher susceptibility to current-induced tilt of the whole OBS.

In the microseismic noise band, peak noise intervals can be attributed to tropical storm activity (cyclones), whereas no clear correlation with cyclones was found at lower frequencies, where tilt and self-noise dominates (20–60 s period band). A possible cause for instrument tilt is the action of ocean-bottom currents, which are predicted to peak in southern winter just like the tilt noise, but global ocean circulation models are not sufficiently constrained to test this hypothesis in more detail.

The RHUM-RUM data set has been assigned FDSN network code YV and will be freely available by the end of 2017. Data and detailed StationXML meta-data files are hosted and served by the RESIF data centre in Grenoble (http://portal.resif.fr/?RHUM-RUM-experiment&lang=en).

Appendix A: Instrument responses

While conceptually straightforward, instrument corrections can be non-trivial in practice because filter description can be complex, and their specifications must exactly match the format expected by the software used to apply the corrections.

A1 Seismometers

Assuming that the seismometer is a causal linear time-invariant system, its response can be described by a series of poles p_m and zeros r_n:

$$G_{\mathrm{inst}}(f) = S_{\mathrm{d,inst}} \cdot A_0 \cdot \frac{\prod_{n=1}^{N}(2\pi i f - r_n)}{\prod_{m=1}^{M}(2\pi i f - p_m)}. \quad \text{(A1)}$$

In Eq. (A1), $S_{\mathrm{d,inst}}$ is the sensitivity at reference frequency f_{r} with dimension counts $(\mathrm{ms}^{-1})^{-1}$. A_0 is a dimensionless normalization constant, which normalizes $G(f)$ to 1 at reference frequency f_{r}. Following convention, we defined $f_{\mathrm{r}} = 1\,\mathrm{Hz} = (2\pi)^{-1}$ ($\mathrm{rad\,s}^{-1}$). The M poles p_m and N zeros r_n describe the frequency-dependency of the response.

Values for each instrument can be queried sending its serial number email to caldoc@guralp.com. Note that these data sheets contain the frequencies of the poles and zeros in Hz, while the StationXML format prefers them in $\mathrm{rad\,s}^{-1}$. All DEPAS seismometers that functioned had the same $M = 4$ poles and $N = 2$ zeros as described in Table A1a, with the exception of RR13 that had $M = 5$ (Table A1b) and RR22 with $M = 6$ poles (Table A1c)[1].

Poles and zeros characterize the first, analogue stage of an instrument; subsequent digital filter stages characterize the ADC (Analogue to Digital Converter) and digital processing units of the data recorder. For the seismometers, the analogue filter stages were obtained from the manufacturers Güralp and Nanometrics, and are compared in Fig. 4.

We follow the SEED reference manual's Appendix C (Ahern et al., 2012) to describe the response $G(f)$ in frequency-domain. The total transfer function is the product of complex response functions for the instrument, ADC and FIR decimation stages:

$$G(f) = G_{\mathrm{inst}}(f) \cdot G_{\mathrm{ADC}}(f) \cdot G_{\mathrm{FIR}}(f). \quad \text{(A2)}$$

The gain or sensitivity $S_{\mathrm{d,inst}}$ is channel specific and is determined by Güralp before delivering the instrument. For our instruments, a typical value is $1980\,\mathrm{V}(\mathrm{ms}^{-1})^{-1}$ with an instrument-specific variance of $15\,\mathrm{V}(\mathrm{ms}^{-1})^{-1}$.

The analogue seismometer signal was converted to digital counts by a SEND GEOLON-MCS data logger. This conversion is assumed to have a flat response curve:

[1]For the 120 s instruments, the manufacturer lists the same 6 poles and 2 zeros as RR22, which is probably not correct, since they describe a corner period of 60 s. But since none of those recorded data, this should not be a problem to users of the data.

Table A1. (a) 4 poles and 2 zeros of the 60 s Güralp CMG-OBS40T used in the German LOBSTER OBS. Can be applied to all 60 s stations but RR13 and RR22. **(b)** 5 poles and 2 zeros of the 60 s Güralp CMG-OBS40T used in station RR13. **(c)** 6 poles and 2 zeros of the 60 s Güralp CMG-OBS40T used in station RR22. **(d)** 11 poles and 6 zeros of the Trillium 240OBS used in the French OBS at RR38, RR50 and RR52. **(e)** 11 poles and 6 zeros of Trillium 240OBS with a serial number below 400. Those were used in stations RR28, RR29, RR31, RR34, RR36 and RR40.

	Pole p_m in $\mathrm{rad\,s}^{-1}$	Zero r_n in $\mathrm{rad\,s}^{-1}$
	(a)	
1/2	$-0.074016 \pm 0.07347\,i$	0
3/4	$-502.65 \pm 596.9\,i$	–
	(b)	
1/2	$-0.074016 \pm 0.074016\,i$	0
3	-502.66	–
4	-1005.3	–
5	-1130.98	–
	(c)	
1/2	$-0.074016 \pm 0.074016\,i$	0
3	-471.24	–
4/5	$-395.1 \pm 850.69\,i$	–
6	-2199.1	–
	(d)	
1/2	$-0.018134 \pm 0.018034\,i$	0
3	-84.4	-72.5
4	$-180.2 + 224.4\,i$	-163.3
5	$-180.2 - 224.4\,i$	-251
6	-725	-3270
7	-1060	–
8	-4300	–
9	-5800	–
10/11	$-4200 \pm 4600\,i$	–
	(e)	
1/2	$-0.017699 \pm 0.017604\,i$	0
3	-85.3	-72.5
4	$-155.4 + 210.8\,i$	-159.3
5	$-155.4 - 210.8\,i$	-251
6	-713	-3270
7	-1140	–
8	-4300	–
9	-5800	–
10/11	$-4300 \pm 4400\,i$	–

$$G_{\mathrm{ADC}}(f) = S_{\mathrm{d,ADC}}. \quad \text{(A3)}$$

The sensitivity of this stage is $S_{\mathrm{d,ADC}} = 3.62 \times 10^5$ counts V^{-1}, resulting in an overall sensitivity for the LOBSTER seismometers of roughly 7.4×10^5 counts $(\mathrm{m\,s}^{-1})^{-1}$ at reference frequency $f_{\mathrm{r}} = 1$ Hz (see Fig. 4).

The decimation of the digital signal to the recording frequency is described by a series of N_{FIR} FIR decimation filters. The kth digital filter stage has L_k coefficients $b_{l,k}$, decimating an input signal of sampling rate Δt_i. The total FIR response is the product of the individual FIR stages:

$$G_{\mathrm{FIR}}(f) = \prod_{k=1}^{N_{\mathrm{FIR}}} S_{\mathrm{d,FIR},k} \sum_{l}^{L_k} b_{l,k} e^{2\pi i \Delta t_k}. \tag{A4}$$

For the DEPAS instruments, the decimation from 512 kHz to 50 or 100 Hz is described by 8 (100 Hz) or 9 (50 Hz) FIR stages of uniform sensitivity $S_{\mathrm{d,FIR},k} = 1$, such that the sensitivity is only affected by the instrument and ADC stages. The coefficients $b_{l,k}$ have been defined by DEPAS and are included in the StationXML and dataless files. They create the sharp cut-off at 90 % of the Nyquist frequency in Figs. 4 and 5.

The INSU Trillium-240OBS seismometers features $M = 12$ poles p_m and $N = 5$ zeros r_n in its analogue stage (see Tables A1d and e). The p_m and r_n were taken from the Trillium-240 user guide, which applies to the 240OBS as well. The sensitivity is $S_{\mathrm{d,inst}} = 598.45\,\mathrm{V(ms^{-1})^{-1}}$. This is half the value specified in the user guide, since the OBS were connected single-ended. The analogue gain is 0.225 for the horizontal channels and 1.0 for the vertical channel, to maximize the vertical sensitivity while avoiding clipping on the horizontal channel. The sensitivity of the CS5321-2 A/D converter is $1\,165\,080\,\mathrm{counts\,V^{-1}}$, resulting in an overall sensitivity of $6.97 \times 10^7\,\mathrm{counts(m\,s^{-1})^{-1}}$ on the horizontal and $1.57 \times 10^8\,\mathrm{counts/(m\,s^{-1})^{-1}}$ on the vertical channels, both at reference frequency $f_{\mathrm{r}} = 1$ Hz. The decimation from 8000 to 62.5 Hz is implemented by 7 FIR stages of uniform sensitivity.

A2 DEPAS hydrophones

The responses of the hydrophones and differential pressure gauges are also given by Eq. (A2), though with a different instrument response $G_{\mathrm{inst,h}}(f)$, that has to be calculated separately for each instrument, as briefly explained here: a hydrophone measures pressure variations via a piezo element, which has a sensitivity of $S_{\mathrm{d,hyd}}$ in $\mathrm{V\,Pa^{-1}}$. Below its corner frequency (typically in the kHz range), its equivalent circuit is a capacitor C_{hyd}. Together with the input capacity of the amplifier C_{amp}, the system has the total capacitance $C_{\mathrm{total}} = \frac{C_{\mathrm{amp}} C_{\mathrm{hyd}}}{C_{\mathrm{amp}} + C_{\mathrm{hyd}}}$. With the input impedance R of the sensor, the system forms a high-pass filter with a transfer function

$$G_{\mathrm{inst,h}}(f) = S_{\mathrm{d,hyd}} \frac{RC_{\mathrm{total}} 2\pi i f}{1 + RC_{\mathrm{total}} 2\pi i f}, \tag{A5}$$

equivalent to Eq. (A1) with a single pole

$$p_1 = -\frac{1}{RC_{\mathrm{total}}} = -\frac{C_{\mathrm{amp}} + C_{\mathrm{hyd}}}{RC_{\mathrm{amp}} C_{\mathrm{hyd}}}\,\mathrm{rad\,s^{-1}} \tag{A6}$$

and one zero $r_1 = 0\,\mathrm{rad\,s^{-1}}$.

The capacitance C_{hyd} is instrument-specific. The reference value from the manufacturer HighTechInc is $C_{\mathrm{hyd}} = 45$ nF. Before sale, every hydrophone is calibrated, which showed a mean value $C_{\mathrm{hyd}} = 56.3$ nF with a sample standard deviation of 3.5 nF amongst the 60 instruments in the DEPAS pool. The input resistance R of the data logger was either 210 or 500 MΩ, depending on the instrument version.

The sensitivity S_{h} is different for each hydrophone, around $185\,\mathrm{\mu V\,Pa^{-1}}$ with a sample standard deviation of $8\,\mathrm{\mu V\,Pa^{-1}}$ amongst the DEPAS instruments. DEPAS supplied us with values for S_{d}, R and C_{hyd} for each instrument. From those, we calculated poles, zeros and sensitivities, which are listed in the dataless SEED and StationXML files available from the RESIF data centre. Geomar instruments were equipped with a similar hydrophone model, HTI-01-PCA from the same manufacturer. Its nominal values is $C_{\mathrm{hyd}} = 50$ nF and since no individually calibrated responses were available, we used the average value of the other HTI-01-PCA in the DEPAS pool, resulting in $S_{\mathrm{d}} = 199.5\,\mathrm{\mu V\,Pa^{-1}}$ and $p_1 = 0.10774\,\mathrm{rad\,s^{-1}}$. This applies to the Geomar OBS (RR33, RR39, RR53 and RR56) as well as to RR45 and RR55, where Geomar hydrophones were attached to LOBSTER OBS.

A3 INSU differential pressure gauges

Differential pressure gauges (DPGs, Cox et al., 1984) are hand-manufactured in research laboratories and their sensitivity and low-pass frequency are challenging to calibrate. The DPGs in stations RR28 and RR29 were manually calibrated on land by comparing their impulse response to that of an absolute pressure gauge in a vacuum jar. Since the low-pass frequency is highly dependent on the viscosity of the oil in the gauge and this viscosity may change with temperature and pressure, it is not sure that these values accurately reflect the instrument response at the seafloor, although visual comparison with the DEPAS hydrophone PPSDs does not suggest significant error. The DPGs on the other sensors were not calibrated and the instrument responses given are therefore the same as those for station RR28. This practice is the same as that used by other OBS facilities (e.g. Godin et al., 2013), but it leaves a significant uncertainty in the converted signal amplitudes.

Appendix B: Description of laboratory experiments on the DEPAS clocks

Since the internal clocks of several DEPAS OBS stopped before retrieval, and ambient noise estimation of the clock error proved impossible, we tried to estimate the clock error

from laboratory experiments. Hence we re-ran several data recorders after their return to the DEPAS lab at AWI Bremerhaven, in an attempt to measure their clock drifts. Only seven data loggers were available (RR06, RR11, RR41, RR43, RR44, RR45, RR55); the remainder had been redeployed in new experiments. Attached to their original lithium batteries and a seismometer, the recorders were run for 7 days, and then for another 33 days. Table B1 shows the skews measured after the two runs, linearly extrapolated to a hypothetical run time of 365 days.

For 6 out of 7 stations, skew values from the two runs agree to within less than 0.1 s. The exception is RR44, where the skews disagree by more than one second (-0.50 s from the 7-day run, versus $+0.55$ s from the 33-day run). For RR11, a skew of $+0.61$ s had been obtained upon OBS recovery (see Table 3), as compared to -0.15 and -0.21 s in the two lab runs (Table B1), which means mutual consistence to within 0.8 s, an uncertainty as large as the skew estimates themselves. No skew upon recovery was available for the remaining six recorders.

Most lab skew values in Table B1 are rather small in magnitude, compared to skews obtained during the field campaign in Table 3. This pattern is consistent with the direct comparison available for RR11, and hints at a systematic difference between seafloor runs and lab runs. In either setting, the clocks tend to run too fast, as indicated by mostly positive skew values (upon recovery, the elapsed recorder time is larger than the elapsed GPS time). But clocks on the seafloor ran even faster than clocks in the lab. (Note that only DEPAS stations in Table 3 should enter this comparison, since INSU recorders are of a different make.)

The likely shortcoming of our lab experiments is that we did not simulate temperature conditions of the real experiment: a sudden drop from 22 to 4 °C) upon deployment, a constant 4 °C during recording, and sudden warming to 22 °C upon recovery. Solid-state oscillators are known to be temperature dependent, which may explain why our lab experiments could match the field observations qualitatively (correct sign of skew), but probably did not yield the correct skew magnitudes. Hence we assign low confidence to the skew measurements in Table B1 and do *not* apply any skew corrections to RHUM-RUM time series based on these values.

Table B1. Lab measurements of clock skews for seven DEPAS recorders. Two separate runs of 7 and 33 days durations yielded skew measurements that are linearly extrapolated to a hypothetical run of 365 days duration (for convenient comparison to skews measured in the field campaign, Table 3). We assign low confidence to these lab measurements (see text for discussion) and do *not* correct RHUM-RUM time series using these values.

Station	Serial number	Skew prediction for 365 days	
	(data logger)	from 7 day exp.	from 33 day exp.
RR06	060744	0.15 s	0.13 s
RR11	060753	−0.15 s	−0.21 s
RR41	050922	0.3 s	0.23 s
RR43	060702	0.00 s	0.033 s
RR44	060751	−0.5 s	0.55 s
RR45	080104	0.045 s	−0.05 s
RR55	060748	0.0015 s	−0.03 s

Appendix C: Summary charts of noise levels across the RHUM-RUM OBS network

Figures C1 to C3 are graphical summaries of noise statistics for all stations and components, in three different frequency bands:

Fig. C1: microseismic noise band (period range 5–15 s). DEPAS and INSU seismometers record comparable noise levels.

Fig. C2: low-noise notch (period band 15–40 s). The noise level of the INSU seismometers is on average 15 dB lower than the values for the DEPAS instruments.

Fig. C3: long-period band (40–100 s). Both INSU seismometers (corner period 240 s) and the DEPAS seismometers (corner period 60 s) still have nominal instrument sensitivity in this band, but the self-noise of the Güralp instruments used in the DEPAS OBS is pronounced, especially on the BHZ channel.

Probabilistic Power Spectral Densities (cf. Fig. 9) were calculated for all stations and broadband components (BH1, BH2, BHZ, BDH) by stacking hour-long time series. For each of the three frequency bands, we averaged the hourly spectra over the frequencies contained the band of interest, and calculated the median, quartiles, 2.5 % percentile, and 97.5 % percentile power levels of the hourly band averages. These statistics are plotted for all stations, components and frequency bands in Figs. C1 to C3.

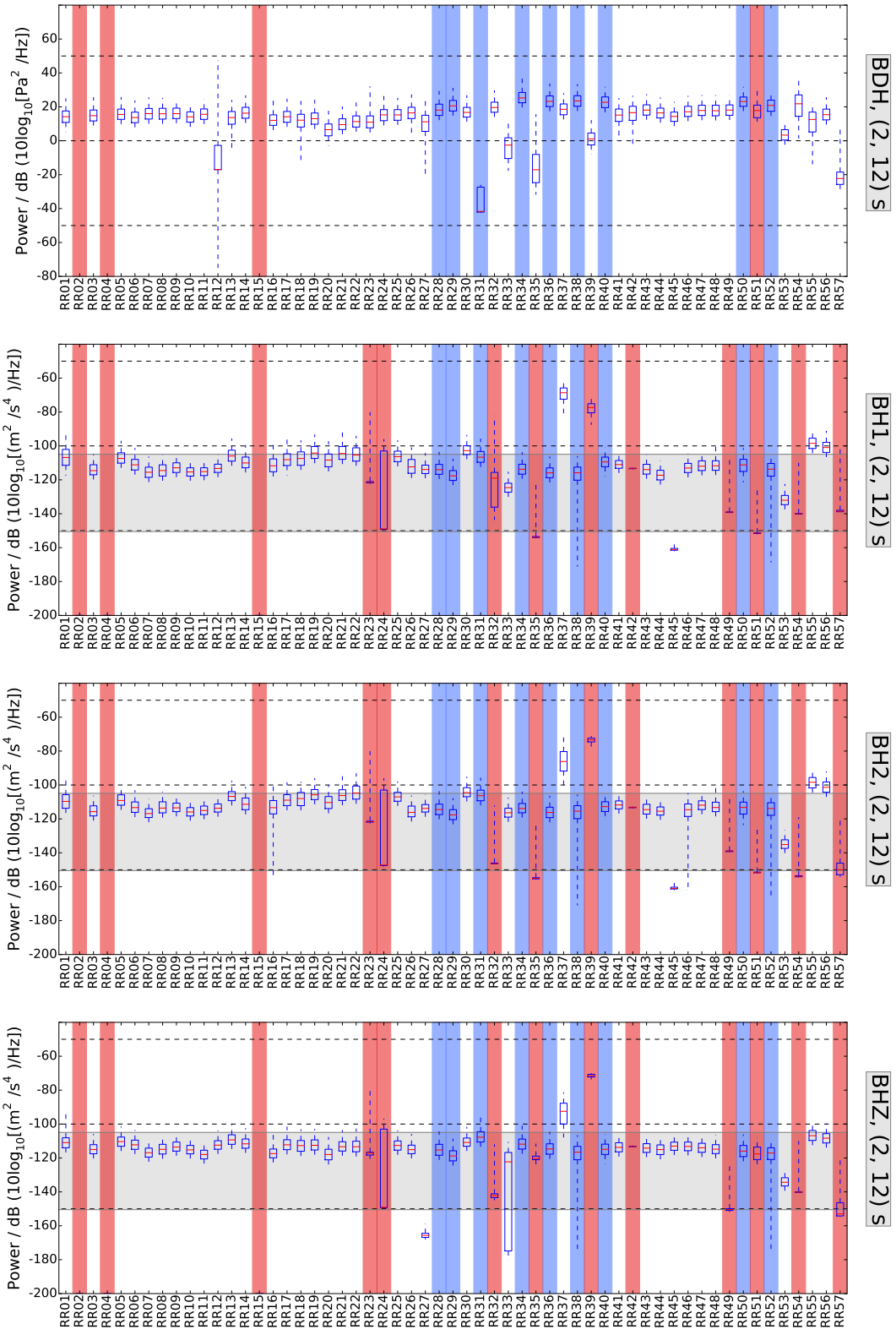

Figure C1. Noise power levels in the microseismic noise band (5–15 s period), on the BH1, BH2, BHZ, and BDH components (4 sub-plots). 57 box plots per panel characterize the 57 RHUM-RUM stations. In each box plot, the red line marks the median power level during the interval of successful recording. Top and bottom edges of the blue box mark the ranges of the two quartiles, and dashed line the range that contains 95 % of all hourly observations in this frequency band (from 2.5 to 97.5 % percentile). Light blue shading indicates INSU stations, all others are DEPAS or Geomar. Red shading indicates failed components. Grey horizontal band marks the power range bracketed by the (terrestrial) New Low Noise and New High Noise Models (Peterson, 1993), in the frequency passband considered here.

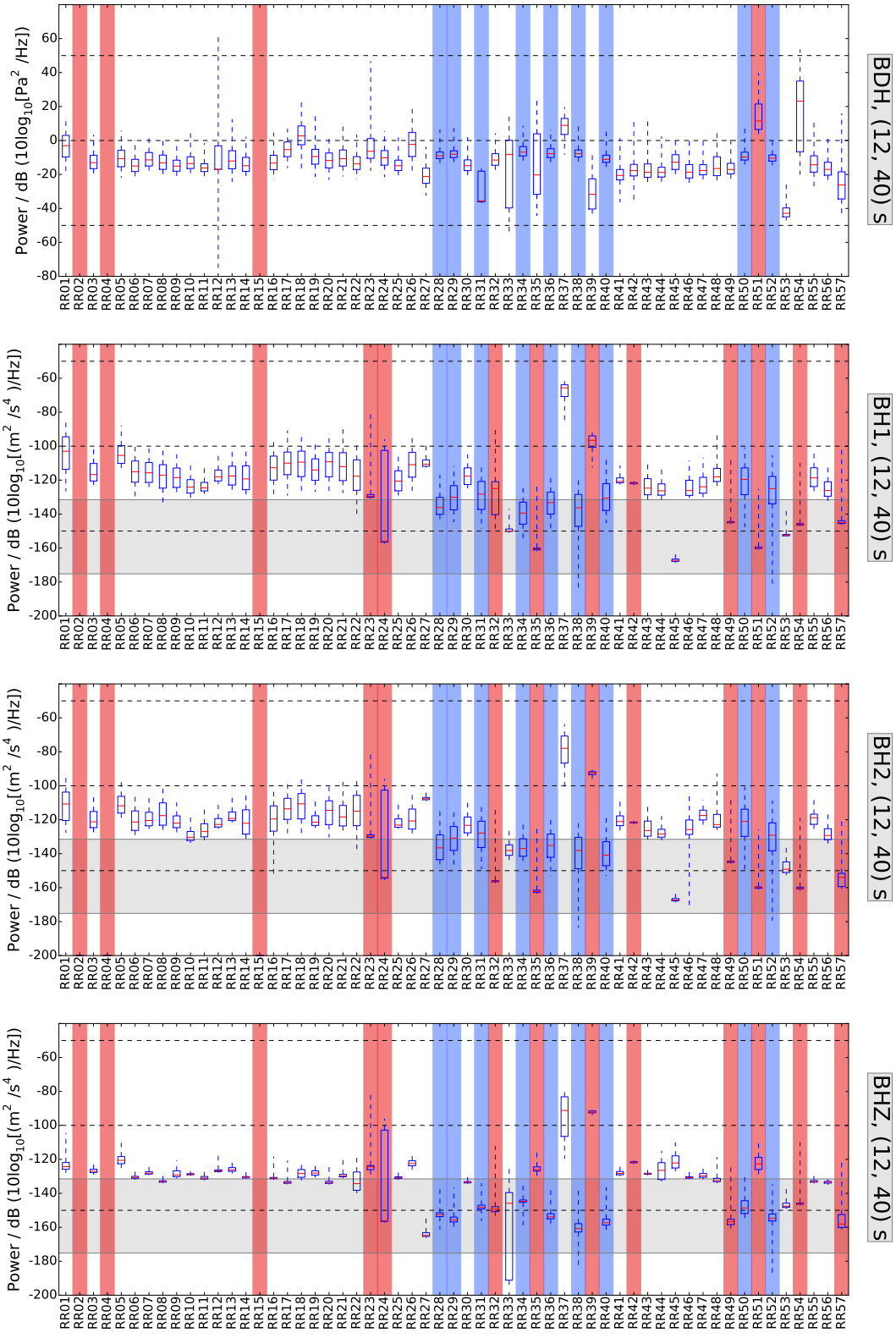

Figure C2. Noise power levels in the band of the low-noise notch (15–40 s period). Refer to the caption of Fig. C1 for explanation.

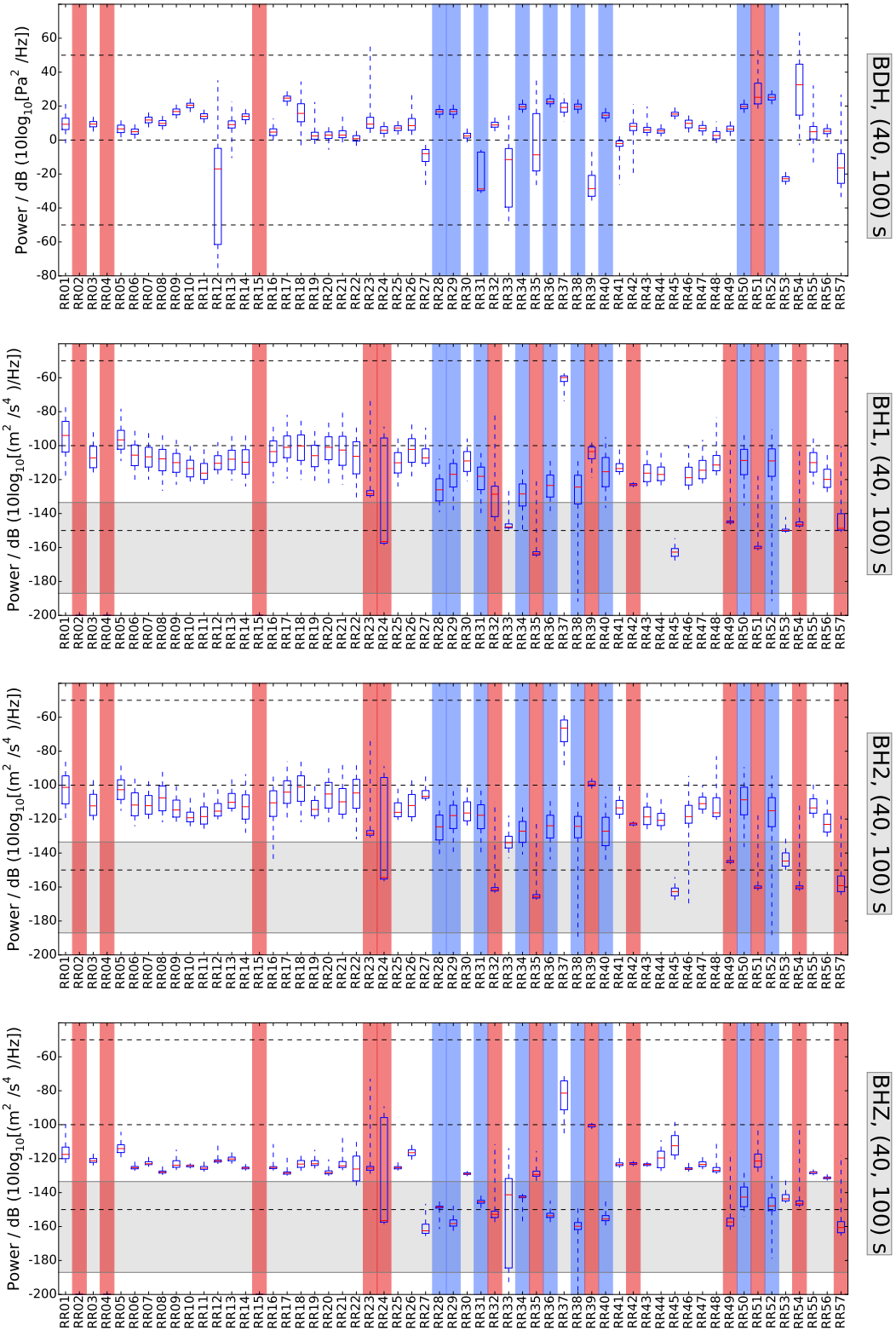

Figure C3. Noise power levels in the long-period band (40–100 s period). Refer to the caption of Fig. C1 for explanation.

The Supplement related to this article is available online at doi:10.5194/adgeo-4-43-2016-supplement.

Author contributions. K. Hosseini, M. Tsekhmistrenko, K. Sigloch, S. C. Stähler, W. C. Crawford, J.-R. Scholz and A. Mazzullo processed raw data and assessed station performance during and after the OBS recovery cruise. Station meta-data were assembled and verified for the DEPAS instruments by S. C. Stähler and M. C. Schmidt-Aursch, and for the INSU instruments by W. C. Crawford. A. Mazzullo, M. Deen and W. C. Crawford investigated the "glitch" on the INSU instruments. G. Barruol and K. Sigloch designed the RHUM-RUM project, obtained funding for the OBS experiment, and led the cruises. S. C. Stähler and K. Sigloch prepared the manuscript with contributions from all co-authors.

Acknowledgements. RHUM-RUM is funded by Deutsche Forschungsgemeinschaft (grants SI1538/2-1 and SI1538/4-1) and Agence National de la Recherche (project ANR-11-BS56-0013). Additional support is provided by Centre National de la Recherche Scientifique-Institut National des Sciences de l'Univers, Terres Australes et Antarctiques Françaises, Institut Polaire Paul Emile Victor, Alfred Wegener Institute Bremerhaven, and a Marie Curie Career Integration Grant to K. Sigloch. Instruments were provided by "Deutscher Geräte-Pool für Amphibische Seismologie" at Alfred-Wegener-Institut, Bremerhaven, "Parc Sismomètre fond du mer" at INSU/IPGP, and Geomar, Kiel. We thank Erik Labahn, Henning Kirk, and the crews of research vessels *Marion Dufresne* and *Meteor* for excellent support during deployment and recovery. We thank Carlos Corela for preparing the initial compilation of the DEPAS metadata. Ulf Gräwe assisted with downloading HYCOM ocean model data (http://hycom.org). All figures were produced with the ObsPy software, version 0.10.2 (The ObsPy Development Team, 2015). We thank the RESIF data centre in Grenoble, especially Catherine Pequegnat and Pierre Volcke, for hosting the RHUM-RUM data.

RESIF is supported by the French Ministry of Education and Research, by 18 Research Institutions and Universities in France, by the French National Research Agency (ANR) as part of the "Investissements d'Avenir" program (reference: ANR-11-EQPX-0040) and by the French Ministry of Ecology, Sustainable Development and Energy.

Edited by: D. Pesaresi
Reviewed by: D. Suetsugu and three anonymous referees

References

Ahern, T. K., Casey, R., Barnes, D., Benson, R., and Knight, T.: Seed Reference Manual, Tech. rep., Incorporated Research Institutions for Seismology, http://www.fdsn.org/media/_s/publications/SEEDManual_V2.4.pdf (last access: 19 October 2015), 2012.

Barruol, G.: PLUME investigates South Pacific Superswell, Eos, Trans. Am. Geophys. Union, 83, 511, doi:10.1029/2002EO000354, 2002.

Barruol, G. and Sigloch, K.: Investigating La Réunion hot spot from crust to core, Eos, Trans. Am. Geophys. Union, 94, 205–207, doi:10.1002/2013EO230002, 2013.

Barruol, G., Sigloch, K., and the RHUM-RUM group: RHUM-RUM experiment, 2011–2015, code YV (Réunion Hotspot and Upper Mantle – Réunion's Unterer Mantel) funded by ANR, DFG, CNRS-INSU, IPEV, TAAF, instrumented by DEPAS, INSU-OBS, AWI and the Universities of Muenster, Bonn, La Réunion, doi:10.15778/RESIF.YV2011, 2011.

Becker, J. J., Sandwell, D. T., Smith, W. H. F., Braud, J., Binder, B., Depner, J., Fabre, D., Factor, J., Ingalls, S., Kim, S.-H., Ladner, R., Marks, K., Nelson, S., Pharaoh, A., Trimmer, R., Von Rosenberg, J., Wallace, G., and Weatherall, P.: Global Bathymetry and Elevation Data at 30 Arc Seconds Resolution: SRTM30_PLUS, Mar. Geodyn., 32, 355–371, doi:10.1080/01490410903297766, 2009.

Cannat, M., Rommevaux-Jestin, C., Sauter, D., Deplus, C., and Mendel, V.: Formation of the axial relief at the very slow spreading Southwest Indian Ridge (49° to 69° E), J. Geophys. Res., 104, 22825, doi:10.1029/1999JB900195, 1999.

Cox, C., Deaton, T., and Webb, S.: A Deep-Sea Differential Pressure Gauge, J. Atmos. Ocean. Tech., 1, 237–246, doi:10.1175/1520-0426(1984)001<0237:ADSDPG>2.0.CO;2, 1984.

Crawford, W. C. and Webb, S. C.: Identifying and Removing Tilt Noise from Low-Frequency (< 0.1 Hz) Seafloor Vertical Seismic Data, Bull. Seismol. Soc. Am., 90, 952–963, doi:10.1785/0119990121, 2000.

Cummings, J. A.: Operational multivariate ocean data assimilation, Q. J. Roy. Meteorol. Soc., 131, 3583–3604, doi:10.1256/qj.05.105, 2005.

Dahm, T., Thorwart, M., Flueh, E. R., Braun, T., Herber, R., Favali, P., Beranzoli, L., D'Anna, G., Frugoni, F., and Smriglio, G.: Ocean bottom seismometers deployed in Tyrrhenian Sea, Eos, Trans. Am. Geophys. Union, 83, 309, doi:10.1029/2002EO000221, 2002.

Davy, C., Barruol, G., Fontaine, F. R., Sigloch, K., and Stutzmann, E.: Tracking major storms from microseismic and hydroacoustic observations on the seafloor, Geophys. Res. Lett., 41, 8825–8831, doi:10.1002/2014GL062319, 2014.

Duennebier, F. K., Blackinton, G., and Sutton, G. H.: Current-generated noise recorded on ocean bottom seismometers, Mar. Geophys. Res., 5, 109–115, doi:10.1007/BF00310316, 1981.

Dyment, J., Lin, J., and Baker, E.: Ridge-Hotspot Interactions: What Mid-Ocean Ridges Tell Us About Deep Earth Processes, Oceanography, 20, 102–115, doi:10.5670/oceanog.2007.84, 2007.

Flueh, E. R. and Biolas, J.: A digital, high data capacity ocean bottom recorder for seismic investigations, Int. Underw. Syst. Des., 18, 18–20, 1996.

Geissler, W. H. and Schmidt, R.: Short Cruise Report Maria S. Merian; MSM 24 Walvis Bay – Cape Town, Tech. rep., Leitstelle Deutsche Forschungsschiffe, Hamburg, https://www.ldf.uni-hamburg.de/merian/wochenberichte/wochenberichte-merian/msm22-msm25/msm24-scr.pdf (last access: 19 October 2015), 2013.

Geissler, W. H., Matias, L., Stich, D., Carrilho, F., Jokat, W., Monna, S., Ibenbrahim, A., Mancilla, F., Gutscher, M. A., Sallars, V., and Zitellini, N.: Focal mechanisms for sub-crustal earthquakes in the Gulf of Cadiz from a dense OBS deployment, Geophys. Res. Lett., 37, 7–12, doi:10.1029/2010GL044289, 2010.

GEOFON: Mw 6.6 earthquake, Sichuan China, 2013-04-20 (Moment Tensor Solution), doi:10.5880/GEOFON.gfz2013hrdy, 2013.

Godin, O. A., Zabotin, N. A., Sheehan, A. F., Yang, Z., and Collins, J. A.: Power spectra of infragravity waves in a deep ocean, Geophys. Res. Lett., 40, 2159–2165, doi:10.1002/grl.50418, 2013.

Gouedard, P., Seher, T., McGuire, J. J., Collins, J. A., and van der Hilst, R.: Correction of Ocean-Bottom Seismometer Instrumental Clock Errors Using Ambient Seismic Noise, Bull. Seismol. Soc. Am., 104, doi:10.1785/0120130157, 2014.

Hannemann, K., Krüger, F., and Dahm, T.: Measuring of clock drift rates and static time offsets of ocean bottom stations by means of ambient noise, Geophys. J. Int., 196, 1034–1042, doi:10.1093/gji/ggt434, 2014.

Laske, G., Collins, J. A., Wolfe, C. J., Solomon, S. C., Detrick, R. S., Orcutt, J. A., Bercovici, D., and Hauri, E. H.: Probing the Hawaiian Hot Spot With New Broadband Ocean Bottom Instruments, Eos, Trans. Am. Geophys. Union, 90, 362–363, doi:10.1029/2009EO410002, 2009.

McNamara, D. E. and Buland, R.: Ambient Noise Levels in the Continental United States, Bull. Seismol. Soc. Am., 94, 1517–1527, doi:10.1785/012003001, 2004.

Meier, T., Friederich, W., Papazachos, C., Taymaz, T., and Kind, R.: EGELADOS: a temporary amphibian broadband seismic network in the southern Aegean, in: Geophys. Res. Abstr., 9, 9020, 2007.

Morgan, W. J.: Rodriguez, Darwin, Amsterdam, …, A second type of Hotspot Island, J. Geophys. Res., 83, 5355, doi:10.1029/JB083iB11p05355, 1978.

Peterson, J.: Observations and Modeling of Seismic Background Noise, Tech. rep., USGS, Albuquerque, New Mexico, 1993.

Ponsoni, L., Aguiar-González, B., Maas, L., van Aken, H., and Ridderinkhof, H.: Long-term observations of the east madagascar undercurrent, Deep-Sea Res. Pt. I, 100, 64–78, doi:10.1016/j.dsr.2015.02.004, 2015.

Scholz, J.-R.: Local seismicity of the segment-8-volcano at the ultraslow spreading Southwest Indian Ridge, Diploma thesis, Technische Universität Dresden, Dresden, 2014.

Sens-Schönfelder, C.: Synchronizing seismic networks with ambient noise, Geophys. J. Int., 174, 966–970, doi:10.1111/j.1365-246X.2008.03842.x, 2008.

Sigloch, K.: Multiple-frequency body-wave tomography, PhD thesis, Princeton, 2008.

Stähler, S. C., Sigloch, K., Barruol, G., and Crawford, W. C.: Noise levels at all stations of the RHUM-RUM OBS network, doi:10.13140/RG.2.1.1374.0886, 2015.

Suetsugu, D., Sugioka, H., Isse, T., Fukao, Y., Shiobara, H., Kanazawa, T., Barruol, G., Schindelé, F., Reymond, D., Bonneville, A., and Debayle, E.: Probing South Pacific mantle plumes with ocean bottom seismographs, Eos, Trans. Am. Geophys. Union, 86, 429, doi:10.1029/2005EO440001, 2005.

Suetsugu, D., Shiobara, H., Sugioka, H., Ito, A., Isse, T., Kasaya, T., Tada, N., Baba, K., Abe, N., Hamano, Y., Tarits, P., Barriot, J.-P., and Reymond, D.: TIARES Project – Tomographic investigation by seafloor array experiment for the Society hotspot, Earth Planets Space, 64, i–iv, doi:10.5047/eps.2011.11.002, 2012.

Sumy, D. F., Lodewyk, J. A., Woodward, R. L., and Evers, B.: Ocean-Bottom Seismograph Performance during the Cascadia Initiative, Seismol. Res. Lett., 86, 1238–1246, doi:10.1785/0220150110, 2015.

The ObsPy Development Team: ObsPy 0.10.2, doi:10.5281/zenodo.17641, 2015.

Tilmann, F., Yuan, X., Rümpker, G., and Rindraharisaona, E.: SELASOMA Project, Madagascar 2012–2014, doi:10.14470/MR7567431421, 2012.

Trehu, A. M.: A note on the effect of bottom currents on an ocean bottom seismometer, Bull. Seismol. Soc. Am., 75, 1195–1204, 1985.

Webb, S. C.: Broadband seismology and noise under the ocean, Rev. Geophys., 36, 105, doi:10.1029/97RG02287,1998.

Wolfe, C. J., Solomon, S. C., Laske, G., Collins, J. A., Detrick, R. S., Orcutt, J. A., Bercovici, D., and Hauri, E. H.: Mantle Shear-Wave Velocity Structure Beneath the Hawaiian Hot Spot, Science, 326, 1388–1390, doi:10.1126/science.1180165, 2009.

Wysession, M., Wiens, D., Nyblade, A., and Rambolamanana, G.: Investigating Mantle Structure with Broadband Seismic Arrays in Madagascar and Mozambique, AGU Fall Meet. Abstr., p. B2591, 2012.